THE MÖSSBAUER EFFECT AND ITS APPLICATION IN CHEMISTRY

E. Fluck

Anorganisch-Chemisches Institut der Universität Heidelberg, Germany

I. Introduction

It has long been believed that the physical behavior of the atomic nucleus is independent of the state of chemical bonding of the atom to which it belongs. That this is not so is shown particularly clearly by the phenomenon of nuclear magnetic resonance (NMR). In 1949, Knight found that the conditions for the nuclear magnetic resonance of the phosphorus nucleus in different phosphorus compounds depended on the way in which the phosphorus atom was bonded (*29*). The same phenomenon was later observed for other isotopes. The differences in behavior, though small, were large enough to form a new type of spectroscopy, nuclear magnetic resonance spectroscopy, which today is among the most important physical aids to chemistry.

In this article another resonance phenomenon of the atomic nucleus, namely, the Mössbauer effect, and its significance for chemistry will be discussed. In this effect, as in nuclear magnetic resonance, the chemical bonding of the atom in question again plays a part.

II. The Mössbauer Effect

The effect discovered by Mössbauer (*33, 34, 35*) and named after him is concerned with the resonance fluorescence of the so-called recoilless γ-radiation of the atomic nucleus.

A. Theory of Resonance Fluorescence

Fluorescence phenomena have been known for a long time. An atom or molecule can be excited by absorption of a sufficiently energy-rich light

quantum $h\nu$, i.e., it can be raised to a higher quantum state (a higher shell). When the atom or molecule reverts from the excited state to the ground state, the absorbed energy is re-emitted as light quanta. If this reversion to the ground state takes place via several quantum states, the energy of the separate light quanta emitted is smaller than that of the incident light quanta. If, however, the atom or molecule is transformed into only the first excited state by the incident quantum, the process of reversion can lead only to the emission of quanta with a single energy, which is equal to that of the quantum absorbed. This special case of fluorescence is termed resonance fluorescence.

A very clear picture of the energy processes involved in resonance fluorescence has been given by Frauenfelder (*14*). Suppose a free atomic or nuclear system of mass m has two energy levels A and B, differing in energy by E_r, as shown in Fig. 1. When the system passes from B to A a

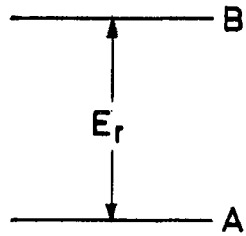

FIG. 1. Energy levels of an atomic or nuclear system: ground state A, first excited state B.

photon with energy E_γ is emitted. It follows from the momentum principle that the momentum p of the photon and the momentum of the atom undergoing recoil, P, must be equal in amount and opposite. If c denotes the velocity of light, the momentum p of the photon is given by Eq. (1):

$$p = \frac{E_\gamma}{c} \tag{1}$$

The recoil energy of the atomic or nuclear system, R, is then

$$R = \tfrac{1}{2}mv^2 = \frac{p^2}{2m} = \frac{P^2}{2m} = \frac{E_\gamma{}^2}{2mc^2} \tag{2}$$

It is assumed that the energy of the photons is negligibly small compared with the rest energy mc^2 of the radiating system, i.e., that the recoil system need not be treated relativistically.

From the law of the conservation of energy, the transition energy E_r

by which the two energy levels A and B are separated must be equal to the sum of the energy of the photon and the recoil energy R, i.e.,

$$E_r = E_\gamma + R \tag{3}$$

Bearing in mind that the recoil energy R is small compared with E_γ, E_γ in Eq. (2) may be replaced by E_r, so that we have

$$R \cong \frac{E_r^2}{2mc^2} \tag{4}$$

If it is assumed that an atom or atomic nucleus is in an excited state B (Fig. 1) and reverts to the ground state A with emission of a photon, the photon may be absorbed when it encounters another atom of the same element and raise it to the excited state. The second atom subsequently reverts to the ground state and emits a photon of the same energy. The processes of absorption and secondary emission are independent of one another.

Considering the energy of the photons emitted by many excited atoms, it is found that they do not all have exactly the same energy. This is a consequence of the Heisenberg uncertainty principle, according to which the product of the uncertainty of the time τ and the uncertainty of the energy Γ is of the order of magnitude of $\hbar$, where $2\pi\hbar = h$, and h is Planck's constant. If τ is the mean life of a state, the uncertainty of the energy Γ is given by

$$\Gamma = \frac{\hbar}{\tau}$$

When τ is very large, i.e., the state is very stable, the energy of the state is sharp. On the other hand if τ is very small, the energy of the state in question is very uncertain, i.e., it cannot be exactly measured. This implies that, for example, the energy of the stable ground state A of an atom is sharp whereas that of the excited state is not sharp. A characteristic energy distribution for the state B is shown in Fig. 2a. The photons emitted in the transition from B to A accordingly show an analogous energy distribution: the emitted line has a "natural width." Its maximum corresponds to an energy of $E_r - R$ (Fig. 2b).

When a photon with energy E_γ and momentum p impinges on another atom of the same element which is at rest, the whole momentum is transferred to it. It undergoes a recoil and the recoil energy R is again given by Eq. (4). This energy must be made available by the photon. In order to raise the atom in question from state A to a state B, the photon must have

the energy $E_r + R$ if the energy difference between the levels is E_r. A resonance phenomenon will then be observed only if at least some of the photons have a sufficiently high energy to reach the energy level B and simultaneously provide energy R for the recoil system. Resonance fluores-

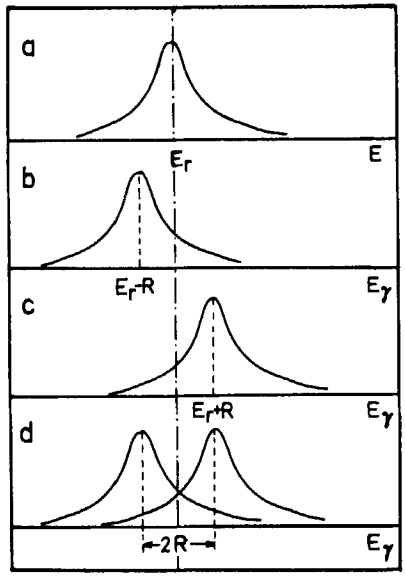

FIG. 2. Energy distribution in resonance fluorescence: (a) energy distribution of the excited state B, (b) energy distribution for the photon emitted in the transition $B \rightarrow A$, (c) energy spectrum for the excitation of the state B *and* providing the energy R, (d) overlapping of (b) and (c) (*14*).

cence will thus occur only if the energy distribution curve for the excitation process (Fig. 2c) and that for the photons available (Fig. 2b) overlap. For this to be the case the line width must be approximately as big, or bigger, than $2R$, i.e.,

$$\Gamma \geqslant 2R$$

Whereas this condition is always satisfied for optical transitions, where transition energies are of the order of 1 ev, it is not in general the case for nuclear transitions with transition energies of the order of 1 kev up to 1 Mev and more.

So far it has been assumed that the radiating and absorbing systems are at rest whereas, in fact, both are in thermal motion. This causes a further broadening of the emission and absorption lines. This broadening

$$D = 2\sqrt{\frac{\overline{P_i^2}R}{2m}} \tag{6}$$

where P_i is the initial momentum of the radiating atom.

The Doppler broadening for optical radiation is very much greater than the recoil energy R. The overlapping of the emission and absorption lines shown in Fig. 2d occurs to a marked extent.

An experimental arrangement for observing resonance fluorescence is shown schematically in Fig. 3. It consists of a source of radiation Q, the

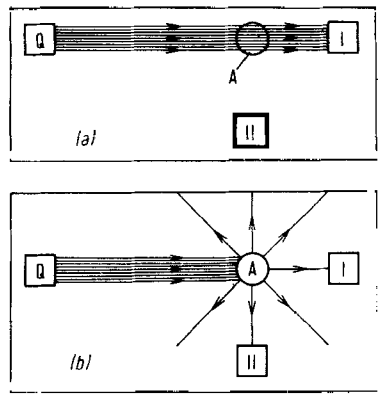

FIG. 3. Schematic representation of resonance fluorescence: (a) no resonance, (b) resonance; Q, radiation source; A, absorber; I and II, radiation detectors.

absorber A, and two detectors I and II. The detectors, which serve to determine radiation intensities, are so placed that one is in the path of the radiation and the other at right angles to it. If the energy of the light quanta emitted from the radiation source does not correspond to that of the first excited state of the atom shell of absorber A, in the sense of what has been said above, no resonance fluorescence will occur. Detector I placed in the path of the beam will then indicate the full intensity passing from the radiation source into the solid angle of the detector, while detector II will receive no radiation (Fig. 3a). If, on the other hand, the energy of the light quanta from Q corresponds to the excitation energy of the first excited state, resonance will occur. The absorber will emit an isotropic radiation which will be observed with detector II (Fig. 3b). The incidence of resonance will be shown by a decrease in the radiation intensity registered by

detector I, and a simultaneous indication of a certain radiation intensity reaching Detector II.

Atoms of the same sort as those which make up the absorber and which are in the requisite excited state will serve as a light source capable of emitting light quanta with the precisely defined energy that is necessary for the excitation of resonance fluorescence. When they revert to the ground state the quanta of the correct energy will be emitted.

B. Nuclear Resonance Fluorescence

All that has been said in the previous section about the conditions for the appearance of fluorescence in the atom is valid in principle for nuclear resonance fluorescence. An atomic nucleus is excited to a suitable energy by irradiation with γ-rays. The γ-radiation emitted from a nucleus in an excited state, like the light coming from the shell, is electromagnetic radiation, so that it should again be possible to observe resonance fluorescence. In general, however, the γ-quanta, because of their substantially higher energy, impart a considerable recoil to the nucleus in the emission process. As a result a considerable part of the excitation energy of the nucleus is lost as recoil energy, and the γ-quantum emitted is consequently too low in energy to excite a nucleus of the absorber.[1] An analogous recoil loss also occurs, as described above, in the absorption process. This recoil loss may be compensated for by imparting to the nucleus prior to the emission of the γ-quantum a velocity in the direction of the absorber, and so securing a Doppler shift of the emitted γ-quantum which corresponds exactly to the expected energy loss. A Doppler shift of $2R$ requires a velocity of E_r/mc. If such a Doppler shift can be attained in any way, nuclear resonance fluorescence can be observed, i.e., a measurable value for the effective cross section (see p. 440) may be obtained. Several methods of obtaining such a Doppler shift have been described. Thus, for example, a Doppler shift of the quantum energy may be secured by mechanical movement of the nucleus, using an ultracentrifuge (for literature, see ref. *35*). Such an experiment was first made in 1950 by Moon (*36*, *37*). He attached a Au^{198} source to the tip of a fast-moving rotor. γ-Quanta emitted tangentially acquired additional energy which was sufficient to compensate for the recoil

[1] The recoil energy for a 14.4-kev γ-quantum which is emitted by an excited iron atom of mass 57 amounts to 1.9×10^{-3} ev from Eqs. (2) or (4), i.e., the γ-quantum (E = 14,400 ev) from an excited Fe^{57} atom has an energy smaller by this amount than the energy difference, E_r, corresponding to the two levels A and B. In general, the recoil energy of a free nucleus of mass number M is given by Eq. (7), where E denotes the γ-ray energy:

$$R \text{ (ev)} \simeq \frac{5.37 \cdot 10^{-4} E^2 \text{ (kev)}}{M} \tag{7}$$

loss. An improved overlap of the absorption and emission lines can be obtained by producing a Doppler broadening by means of an increase in temperature (for literature, see ref. *35*). Finally, earlier emission and absorption processes, such as a β decay preceding the γ transition or the capture of a particle can bring about a Doppler broadening or a Doppler shift of the quantum energy (for literature, see ref. *35*).

The effects produced by such methods are, however, very small since only a minute fraction of the atoms will have exactly the right velocity. This is even more true as the relative line width is generally much smaller than for the lines in optical spectra. In the latter case the energy of the quanta emitted from the radiation source is often within the line width, even if it is reduced by such small energy losses due to recoil, i.e., it still suffices to excite the orbital electron of the absorbing atom. In contrast to this, the finite line width of the γ lines of nuclei is much smaller.

In the Mössbauer effect, the recoil loss is not compensated but avoided altogether. Thus if the emitting atom is incorporated firmly in a suitable crystal lattice, the recoil momentum is taken up by the whole crystal and practically no energy loss occurs provided lattice vibrations are not excited during emission. The resonance criterion is thus satisfied directly for these recoil-free quanta and, in principle, experiments analogous to those for optical resonance fluorescence may be carried out, as shown diagrammatically in Fig. 3a. Resonance can be destroyed if a velocity is given to the radiation source relative to the absorber: this produces a change in energy of the γ-quanta (Doppler shift). If the first energy level of the atomic nucleus of the absorber is shifted for some reason to higher or lower values, so that the energy needed for excitation is somewhat smaller or greater than the energy of the γ-quantum from the radiation source, source and absorber must be set in motion relative to one another for resonance to occur. The requisite velocities are very small. If resonance absorption is observed, i.e., is picked up by detector I in Fig. 3b, the characteristic intensity distribution shown in Fig. 4 will be obtained for the recorded radiation as a function of the velocity of the absorber relative to the radiation source.

The classical experiments on optical and conventional nuclear resonance fluorescence were in general scattering experiments. The true Mössbauer effect, on the other hand, usually involves a study of transmission of γ-rays. The intensity of these transmitted rays is much greater than that of the scattered radiation, and this simplifies the measurement as well as making it more accurate. For nuclei with high conversion coefficients α (see p. 444) the intensity of the scattered radiation is further reduced, since only a fraction $1/(1 + \alpha)$ of the absorbed γ-radiation is re-emitted.

Not all atoms incorporated in a lattice are able to emit the type of recoil-free γ-quanta under discussion, for lattice vibrations are excited to

some extent and some of the energy of the quantum is lost as vibrational energy in this case. The magnitude of the Mössbauer effect thus depends on the proportion of recoil-free quanta to the total intensity, the so-called

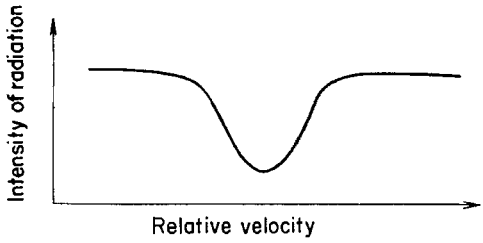

FIG. 4. Intensity of radiation received by detector I as a function of the relative velocity of the radiation source and absorber.

Debye-Waller factor. The effect is greater the smaller the probability of exciting lattice vibrations; i.e., the smaller the γ-quantum energy, the lower the temperature of the crystal and the firmer the bonding of the atom in the lattice.

If it is assumed that there is only one absorbency or scattering level and that the width of the level is determined only by the decay process, the effective cross section[2] for the absorption and scattering process with thin absorbers is given by Eqs. (8) and (9):

$$\sigma_{\text{absorbing}} = \sigma_0 \frac{\Gamma_\gamma \Gamma}{4(E - E_r)^2 + \Gamma^2} \tag{8}$$

$$\sigma_{\text{scattering}} = \sigma_0 \frac{\Gamma_\gamma{}^2}{4(E - E_r)^2 + \Gamma^2} \tag{9}$$

where E is the energy of the γ-ray, Γ the total width of the absorption line, Γ_γ its γ-ray width, and σ_0 the maximum resonance cross section. The last magnitude is given by Eq. (10)

$$\sigma_0 = \frac{2I_B + 1}{2I_A + 1} \cdot 2\pi\lambda^2 \tag{10}$$

where $2\pi\lambda^2$ is the wavelength, I_A the spin of the ground state, and I_B the spin of the excited state. The maximum cross section σ_0 would be observed if the incident γ-rays had energy E_r with a small line width relative to Γ and

[2] The yield of a nuclear process in atomic physics is often expressed in terms of the effective cross section of the nucleus concerned. It depends on the kinetic energy of the exciting particle or, in our case, on the energy of the γ-quantum. The effective cross section denotes the area which the nucleus must possess if each particle collision or each γ-quantum is to lead to a nuclear transformation or to nuclear excitation. Effective cross sections are often expressed in units of 10^{-24} cm^2. This unit is called 1 barn.

if the conversion coefficient were zero. With the above provisos the energy distributions of the absorption and scattering cross sections have a Lorentz shape, as shown in Fig. 2.

Mössbauer discovered the effect with Ir^{191} nuclei, the quantum energy of which is 129 kev. The radiation source was Os^{191}. This decays according to the scheme shown in Fig. 5, with a half-life of 16 days with emission of β-rays, into the second excited state of Ir^{191}. This passes over with emission

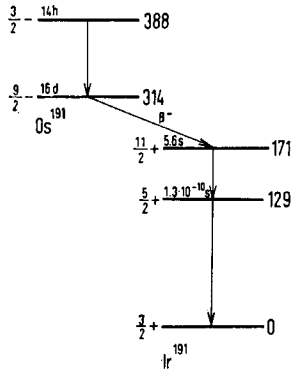

FIG. 5. Decay scheme for $Os^{191} \rightarrow Ir^{191}$.

of a 42-kev γ-quantum into the first excited state, which interests us here. This has a life of 1.4×10^{-10} sec. The ground state is reached by the emission of the 129 kev γ-quantum. Ground state Ir^{191} nuclei in the absorber are excited by these γ-quanta and then revert to the ground state with emission of the fluorescent radiation.

In transmission measurements the γ-quanta arising from the fluorescence radiation are generally ignored. For very exact studies, however, it is necessary to take into account this secondary radiation, which depends on the conversion coefficient and the solid acceptance angle of the photomultiplier detector.

Another measurement made by Mössbauer must also be mentioned, namely, the observation of the temperature effect (*33*). In this case both the source and the absorber were at rest, the latter at a fixed temperature of 88°K and the former at temperatures which could be varied from 88°K to room temperature. He measured the transmission of 129-kev γ-quanta through the absorber as a function of the source temperature. His results are shown graphically in Fig. 6 in terms of the effective absorption cross section. The rise in effective cross section with decreasing temperature (which is quite the reverse of the behavior with gaseous sources and absorbers) was interpreted as due to an increase in the probability of recoil-free emission by the nucleus in the source with decreasing temperature.

TABLE I

PHYSICAL DATA ON ATOMIC NUCLEI[a,b]

Nucleus	Natural abundance (%)	E (kev)	$T_{1/2}$ (sec)	Q	α (e/γ)	R (10^{-2} ev)	σ'_0 (10^{-19} cm^2)	Effect
Fe^{57}	2.17	14.4	$1.0 \cdot 10^{-7}$	$3.2 \cdot 10^{12}$	9.5	0.19	23	X
Ni^{61}	1.25	71	$5.2 \cdot 10^{-9}$	$8.1 \cdot 10^{11}$	K 0.11	4.4	6.6	X
Zn^{67}	4.11	93	$9.4 \cdot 10^{-6}$	$1.9 \cdot 10^{15}$	K 0.63	6.9	1.2	X
Ge^{73}	7.67	13.5	$4 \cdot 10^{-6}$	$1.1 \cdot 10^{14}$	3600	0.13	0.022	—
Kr^{83}	11.55	9.3	$1.5 \cdot 10^{-7}$	$3.1 \cdot 10^{12}$	10	0.055	21.0	X
Ru^{99}	12.7	89	—	—	—	4.3	1.0	—
Ru^{101}	17.0	127	$1.4 \cdot 10^{-9}$	$3.9 \cdot 10^{11}$	K 0.4	8.5	0.97	—
Ag^{107}	51.35	93	44.3	$9.0 \cdot 10^{21}$	16	4.3	0.67	—
Ag^{109}	48.65	88	39.2	$7.6 \cdot 10^{21}$	14	3.8	0.85	—
Sn^{117}	7.57	161	—	—	K 0.13	12.0	1.7	—
Sn^{119}	8.58	24	$1.9 \cdot 10^{-8}$	$1.0 \cdot 10^{12}$	7.3	0.26	10.0	X
Sb^{123}	42.75	161	$6 \cdot 10^{-10}$	$2.1 \cdot 10^{11}$	—	11.0	0.71	—
Te^{123}	0.87	159	$1.9 \cdot 10^{-10}$	$6.6 \cdot 10^{10}$	K 0.17	11.0	1.7	—
Te^{125}	6.99	35	$1.6 \cdot 10^{-9}$	$1.2 \cdot 10^{11}$	K 12	0.52	3.1	X
I^{127}	100	59	—	—	K 2.7	1.5	2.5	—
I^{129}	unstable	26.8	$1.85 \cdot 10^{-8}$	$1.1 \cdot 10^{12}$	5	0.30	25.6	X
Xe^{129}	26.44	40	$7 \cdot 10^{-10}$	$6.2 \cdot 10^{10}$	K 7.5	0.67	30.0	X
Xe^{131}	21.18	80	$4.8 \cdot 10^{-10}$	$8.4 \cdot 10^{10}$	K 1.73	2.6	0.70	—
Cs^{133}	100	81	$6.0 \cdot 10^{-9}$	$1.1 \cdot 10^{12}$	K 1.5	2.7	1.1	—
La^{137}	unstable	10	$8.9 \cdot 10^{-8}$	$2.0 \cdot 10^{12}$	140	0.039	1.3	—
La^{139}	99.9	163	$1.5 \cdot 10^{-9}$	$5.4 \cdot 10^{11}$	K 0.22	10.0	0.56	—
Nd^{145}	8.29	67	$3.3 \cdot 10^{-8}$	$4.8 \cdot 10^{12}$	K 3.3	1.7	0.63	—
	—	72	$<1 \cdot 10^{-9}$	—	K 3.3	1.9	0.82	—
Sm^{149}	13.8	22	$>2.8 \cdot 10^{-9}$	—	—	0.17	—	X
Sm^{152}	26.63	122	$1.4 \cdot 10^{-9}$	$3.7 \cdot 10^{11}$	K 0.7	5.3	4.8	—
Eu^{151}	47.77	22	$9.5 \cdot 10^{-9}$	$4.5 \cdot 10^{11}$	L 12	0.17	5.2	—
Eu^{153}	52.23	84	—	—	—	2.5	4.6	—
	—	97	$<1 \cdot 10^{-9}$	—	K 0.3	3.3	2.0	—
	—	103	$3.4 \cdot 10^{-9}$	$7.7 \cdot 10^{11}$	K 1.2	3.7	0.70	—
Gd^{154}	2.15	123	$1.2 \cdot 10^{-9}$	$3.2 \cdot 10^{11}$	1.5	5.3	3.2	—
Gd^{155}	14.7	60	—	—	—	1.2	10.0	—
	—	87	—	—	K 0.4	2.6	2.3	X
	—	105	—	—	—	3.8	3.3	—
Gd^{156}	20.47	89	$2 \cdot 10^{-9}$	$3.9 \cdot 10^{11}$	K 1.0	2.7	7.7	—
Gd^{160}	21.9	75	—	—	—	1.9	22.0	—
Tb^{159}	100	58	$3.5 \cdot 10^{-11}$	$4.5 \cdot 10^{9}$	K 6.	1.1	1.5	—
	—	137	$5.4 \cdot 10^{-11}$	$1.6 \cdot 10^{10}$	—	6.3	2.6	—
Dy^{160}	2.294	87	$1.8 \cdot 10^{-9}$	$3.4 \cdot 10^{11}$	K 1.5	2.6	6.4	—
Dy^{161}	18.88	25.7	$2.8 \cdot 10^{-8}$	$1.6 \cdot 10^{12}$	—	0.22	37.0	X
	—	49	—	—	—	0.8	6.8	—
	—	74.5	$3 \cdot 10^{-9}$	$4.9 \cdot 10^{11}$	K 0.46	1.8	2.0	X
Dy^{162}	25.53	81	$3.2 \cdot 10^{-9}$	$5.7 \cdot 10^{11}$	—	2.2	19	—
Dy^{163}	24.97	75	—	—	—	1.8	5.8	—
Dy^{164}	28.18	73	$3.5 \cdot 10^{-9}$	$5.6 \cdot 10^{11}$	K 2.7	1.7	6.2	—
Hp^{165}	100	95	$3.3 \cdot 10^{-11}$	$6.9 \cdot 10^{9}$	K 1.77	2.9	1.2	—
Er^{164}	1.56	91	$1.4 \cdot 10^{-9}$	$2.8 \cdot 10^{11}$	K 1.9	2.7	5.1	—
Er^{166}	33.4	80	$1.8 \cdot 10^{-9}$	$3.2 \cdot 10^{11}$	K 1.7	2.1	7.1	X

TABLE I (*Continued*)

Nucleus	Natural abundance (%)	E (kev)	$T_{1/2}$ (sec)	Q	α (e/γ)	R (10^{-2} ev)	σ'_0 (10^{-19} cm²)	Effect
Er^{168}	27.07	79.8	$1.84 \cdot 10^{-9}$	$3.2 \cdot 10^{11}$	K 2.1	2.0	6.2	—
Tm^{169}	100	108.4	$4 \cdot 10^{-9}$	$7.4 \cdot 10^{10}$	—	0.022	700	X
	—	118	$5 \cdot 10^{-11}$	$1.3 \cdot 10^{10}$	K 0.7	4.4	3.1	—
Yb^{170}	3.03	84.2	$1.57 \cdot 10^{-9}$	$2.9 \cdot 10^{11}$	K 1.6	2.2	6.6	X
Yb^{171}	14.31	66.7	$<5 \cdot 10^{-7}$	—	—	1.4	11.0	—
Yb^{172}	21.82	78.7	—	—	—	1.9	20.0	—
Yb^{173}	16.13	78.7	—	—	—	1.9	5.2	—
Yb^{174}	31.84	76.5	—	—	—	1.8	21.0	—
Lu^{175}	94.4	113.8	$8 \cdot 10^{-11}$	$2.0 \cdot 10^{10}$	K 1.6	4.0	0.90	—
Hf^{176}	5.21	88.3	$1.35 \cdot 10^{-9}$	$2.6 \cdot 10^{11}$	K 1.32	2.4	6.7	—
Hf^{177}	18.5	113	$4.2 \cdot 10^{-10}$	$1.0 \cdot 10^{11}$	K 0.75	3.9	1.4	X
Hf^{178}	27.1	93.1	$1 \cdot 10^{-9}$	$2.0 \cdot 10^{11}$	—	2.6	14.0	—
Hf^{180}	35.22	93	$1.4 \cdot 10^{-9}$	$2.9 \cdot 10^{11}$	KL 4.0	2.6	2.8	—
Ta^{181}	100	6.25	$6.8 \cdot 10^{-6}$	$9.4 \cdot 10^{13}$	44	0.012	17	—
	—	136.1	$5.7 \cdot 10^{-11}$	$1.7 \cdot 10^{10}$	K 1.5	5.5	0.66	X
W^{180}	0.135	102	—	—	5	3.1	2.0	—
W^{182}	26.4	100	$1.3 \cdot 10^{-9}$	$2.9 \cdot 10^{11}$	4.5	2.9	2.2	X
W^{183}	14.4	46.5	—	—	9	0.63	2.3	X
	—	99.1	$5.2 \cdot 10^{-10}$	$1.1 \cdot 10^{11}$	3.5	2.9	1.7	X
W^{184}	30.6	111	$1.3 \cdot 10^{-9}$	$3.2 \cdot 10^{11}$	K 0.99	3.6	5.0	—
W^{186}	28.4	123	$1.0 \cdot 10^{-9}$	$2.7 \cdot 10^{11}$	K 0.45	4.4	5.6	—
Re^{185}	37.07	125	—	—	K 2.4	4.5	0.61	—
Re^{187}	62.93	134	$2 \cdot 10^{-9}$	$5.9 \cdot 10^{11}$	K 2.1	5.2	0.58	X
Os^{186}	1.59	137	$5.1 \cdot 10^{-10}$	$1.5 \cdot 10^{11}$	K 0.45	5.4	4.5	—
Os^{188}	13.3	155	$6.2 \cdot 10^{-10}$	$2.1 \cdot 10^{11}$	K 0.40	6.8	3.6	—
Os^{189}	16.1	69.5	—	—	—	1.4	—	—
Os^{190}	26.4	187	$3.5 \cdot 10^{-10}$	$1.4 \cdot 10^{11}$	K 0.2	9.9	2.9	—
Os^{192}	41.0	206	$2.8 \cdot 10^{-10}$	$1.3 \cdot 10^{11}$	K 0.16	12.0	2.5	—
Ir^{191}	38.5	82.6	$3.9 \cdot 10^{-9}$	$7.1 \cdot 10^{11}$	—	1.9	1.8	—
	—	129	$1.4 \cdot 10^{-10}$	$4.0 \cdot 10^{10}$	K 2.9	4.7	0.56	X
Ir^{193}	61.5	73	$6 \cdot 10^{-9}$	$9.6 \cdot 10^{11}$	—	1.5	2.3	X
	—	139	$1.0 \cdot 10^{-9}$	$3.1 \cdot 10^{11}$	K 2.2	5.4	0.59	—
Pt^{195}	33.8	99	$1.4 \cdot 10^{-10}$	$3.0 \cdot 10^{10}$	9.0	2.7	0.50	X
	—	129	$5.5 \cdot 10^{-10}$	$1.6 \cdot 10^{11}$	—	4.6	4.4	—
Au^{197}	100	77	$1.9 \cdot 10^{-9}$	$3.2 \cdot 10^{11}$	2.5	1.6	0.59	X
Hg^{199}	16.84	158	$2.4 \cdot 10^{-9}$	$8.3 \cdot 10^{11}$	K 0.2	6.7	2.4	—
Hg^{201}	13.22	32.1	—	—	—	0.27	24.0	—
	—	167.6	$<2 \cdot 10^{-9}$	—	K 1.5	7.5	0.18	—

[a] From Frauenfelder (*14*) and personal communication.

[b] Q = ratio of γ-ray energy $E\gamma$ to line width $\Gamma = \hbar \ln 2/T_{1/2}$.

α = total internal conversion coefficient (K implies α_K, L implies α_L).

R = recoil energy of free nucleus in units of 10^{-2} ev.

σ'_0 = Mössbauer absorption cross section in units of 10^{-19} cm², calculated with the listed values of the conversion coefficient and assuming natural line width. In the case of an unknown conversion coefficient the cross section has been calculated by assuming $\alpha = 0$. Once α is known, the correct cross section can be found by multiplying the value in the table by $1/(1 + \alpha)$.

X = an effect has been observed.

Mössbauer was able to explain these results quantitatively by modifying a theory due to Lamb (*30*), which dealt with the resonance absorption of neutrons by nuclei fixed in a crystal lattice. Mössbauer applied this theory to the γ-resonance process.

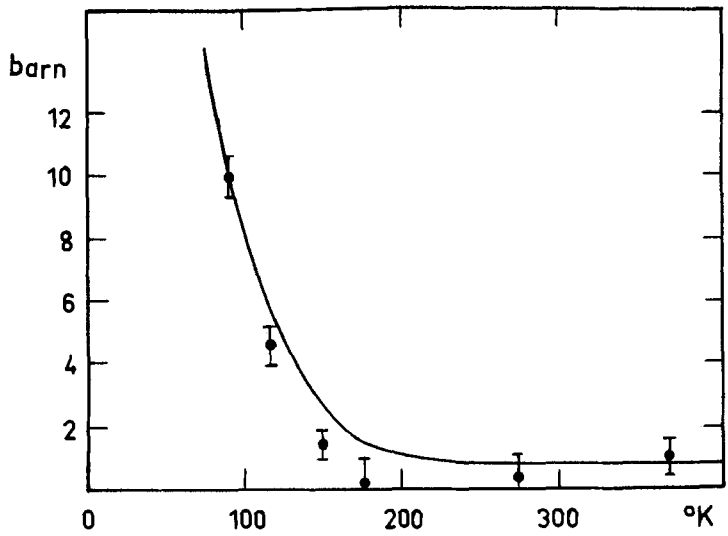

FIG. 6. Effective cross section per Ir^{191} nucleus (temperature of absorber, 88°K).

Table I shows the isotopes known at present for which the Mössbauer effect has been observed or which appear to be suitable for this purpose. It is, however, certainly correct to assume that other isotopes will be found in the future which will be useful for the type of investigation described in this article. The isotope Fe^{57} has proved to be particularly suitable for the study of effects due to the nature of the chemical bonding of the atom, which is dealt with in what follows.

Excited Fe^{57} results from the decay of Co^{57} (cf. decay scheme, Fig. 7). The energy of the quantum is 14.4 kev, the halflife of the first excited state is 1.0×10^{-7} sec, and the derived line width is 4.6×10^{-9} ev. Velocities needed for measurements of the line width are of the order of some tenths of a millimeter per second, a velocity of 0.1 mm/sec corresponding to an energy of 4.8×10^{-9} ev.

In principle such studies are possible for all nuclei with a low-energy first excited state, a sufficiently small line width, and a sufficiently small conversion coefficient α. The conversion coefficient α gives the ratio of the decays by internal conversion with resultant electron emission to one by γ-quanta. When internal conversion occurs instead of emission of a γ-quantum, the nucleus is able to return to the ground state when an electron in

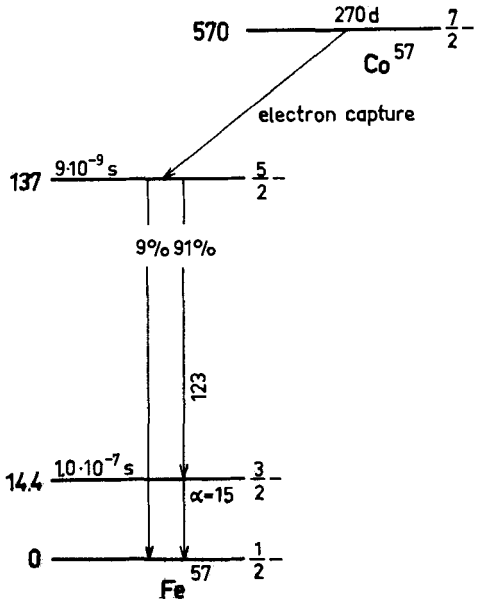

FIG. 7. Decay scheme for $Co^{57} \rightarrow Fe^{57}$.

the inner shell takes up the excitation energy and leaves the atom. Such conversion is particularly large for small γ energies. With Fe^{57} the conversion coefficient for the 14.4-kev level is about 9.5. The total line width Γ and the γ-ray line width Γ_γ, are related by Eq. (11)

$$\frac{\Gamma_\gamma}{\Gamma} = \frac{1}{1+\alpha} \tag{11}$$

Finally, the nuclear spin should not be greater than $\frac{3}{2}$, as the structure of the spectrum is otherwise very complex and difficult to resolve. If the isotopes in Table I are considered from this point of view, it will be seen that Sn^{119} is very suitable, in addition to Fe^{57}. Nuclei such as Ni^{61}, Zn^{67}, Xe^{129}, Dy^{161}, Tm^{169}, Ta^{181}, Pt^{195}, and Au^{197} are also useful.

III. Applications of the Mössbauer Effect

A. Physical Applications

One of the possible applications of the Mössbauer effect in nuclear physics is the determination of the life of an energy state from the line width of the resonance and the measurement of the magnitude of the effect as a function of various factors. The line width Γ may be determined readily

and the life of the state may then be calculated from Eq. (13). If the line width is expressed in ev, the mean life τ is given by:

$$\tau \text{ (sec)} = \frac{6.58 \times 10^{-16}}{\Gamma(\text{ev})} \tag{13}$$

or the half life, $T_{1/2}$ by:

$$T_{1/2} \text{ (sec)} = \frac{4.55 \times 10^{-16}}{\Gamma(\text{ev})} \tag{14}$$

The relationship between mean life and half life of a state is $T_{1/2} = \tau \ln 2 = 0.6931\,\tau$. Thus, for example, Mössbauer found for the mean life of the 129-kev level of Ir^{191} a value of $\tau = 1.0 \times 10^{-10}$ sec, and for the 134-kev level of Re^{187} $\tau = (1.5 \pm 0.2) \times 10^{-11}$ sec.

Earlier electronic measurements had given a mean life of $\tau = 1.4 \times 10^{-7}$ sec for the excited state of Fe^{57}, corresponding by Eq. (13) to a line width Γ of 4.7×10^{-9} ev. Using the narrow lines of Fe^{57} (ratio of line width to quantum energy about $1:10^{12}$) it was further shown, for example, that the small energy shifts of γ-quanta in the gravitational field could be detected, i.e., it was shown that the γ-quanta had altered in energy by a certain amount after falling through a certain height in the earth's gravitational field (*41*).

Finally, it is possible to use the Mössbauer effect to measure directly the Zeeman effect, i.e., the splitting of excited states in a magnetic field, which is very small for nuclei because of their small magnetic moments (*17*). Thus the resonance line of Fe^{57} was split into six components (cf. Figs. 13 and 14). The very strong magnetic field needed to produce this splitting is produced by the crystal field and orbital electrons. The nuclear magnetic moments or the field strength at the nucleus could be deduced from the magnitude of the splitting.

B. Chemical Applications

The possibility of using the Mössbauer effect in chemistry arises from the observation that the position and shape of the resonance line depend on the chemical bonding of the atom to which the nucleus in question belongs in ways to be discussed fully later. Since the properties of the iron isotope Fe^{57} are particularly favorable for the precise study of the Mössbauer effect, the phenomena of isomer shift, quadrupole interaction and temperature shift, described in the following sections, were first studied in detail with this isotope. Points of chemical interest arising from the results are discussed and analogous studies with Sn^{119} are reported in Section III,B,*10*.

1. Methods of Measurement

The substance to be studied is used in the measurements as a resonance absorber, and its transmission is observed as a function of the relative velocity of the absorber and source. In measuring the transmission of the resonance absorber, it is important to have automatic recording of the whole velocity spectrum as well as a sufficient over-all accuracy. In this connection the method which was first used by Ruby *et al.* (*46*) is coming increasingly into use with various modifications. The source (or the absorber) is set into vibration by means of a loud-speaker, the instantaneous velocity being measured with a coil in a homogeneous magnetic field. The γ pulses are recorded as a function of the velocity in a multichannel analyzer. Figure 8 shows diagrammatically a typical setup for making the measurement (*24*).

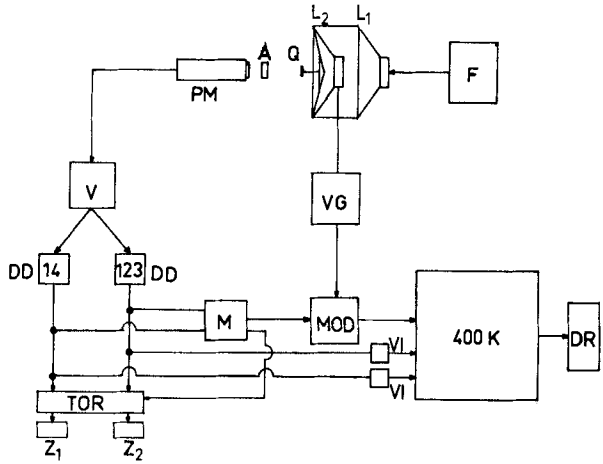

FIG. 8. Diagram of the assembly for measuring the Fe^{57} Mössbauer effect: Q, Co^{57} source; A, resonance absorber; PM, γ-detector (photomultiplier); VI, pulse amplifier; DD 14 and DD 123, differential discriminators; M, pulse-mixer system; Z_1 and Z_2 counters; F, low frequency generator; L_1 driver loud-speaker; L_2, measurement loud-speaker; VG, direct current amplifier; MOD, modulator; 400-K, multichannel pulse-height analyzer (kicksorter); V, variable delay line; DR, recorder.

Two acoustically coupled loud-speakers, L_1 and L_2, are used as velocity drive and for measuring the velocity. The γ-quanta emitted by the Co^{57} source after passage through the resonance absorber reach a 1-mm thick NaI(Tl) crystal and are recorded by a photomultiplier PM. The pulse leaving the detector is fed through a pulse amplifier to differential discriminators, where the pulses of the 14.4-kev and 123-kev γ-radiation are separated. The solid angle of the detector (1%) is defined by a lead diaphragm. The driver loud-speaker L_1, which is fed by the generator F, sets

the membrane of the loud-speaker L_2 in vibration acoustically with the resonance frequency of approximately 30 cycles/sec. The Co^{57} source Q is rigidly linked with the voice coil of L_2. The mechanical mounting of the loud-speaker used for the measurement must be very stable so as to eliminate vibrations. The voltage induced in the voice coil of the measuring loud-speaker L_2, which is proportional to the instantaneous velocity, serves, after it has been amplified in a broad-band direct-current amplifier VG, as a means of modulating the detector output pulses, the height of the pulse thus becoming a linear function of the velocity. Figure 9 shows the principle

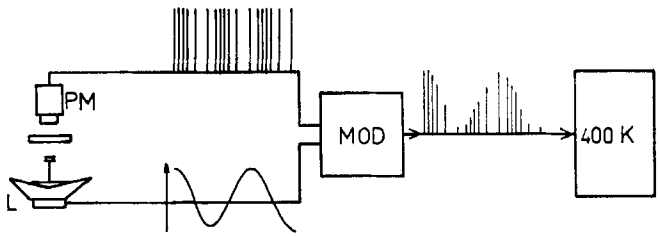

FIG. 9. Operation of modulator. Pulses from the photomultiplier PM are modulated through the velocity spectrum in the modulator MOD and then fed into the multichannel pulse-height analyzer, 400-K. The source is mounted on the coil of loud-speaker L.

of the modulation procedure. The pulses of the photomultiplier PM are modulated in the modulator MOD by the velocity spectrum $v(t)$ and then fed to the multichannel pulse height analyzer.

The modulator MOD deals with the 14.4-kev and 123-kev pulses from the pulse mixer system M, which are fed after modulation to a 400-channel pulse-height analyzer. The record of the intensity of the 14.4-kev radiation is stored in the first half and that of the 123-kev radiation in the second half of the multichannel analyzer as a function of the velocity. Distribution between the two halves is secured by a gate signal from the 123-kev pulses, the delay of which is arranged so that the positions of the channels are the same for both halves. The U-form velocity distribution resulting from the sinusoidal movement is eliminated by normalization of the 14.4-kev resonance radiation with respect to the 123-kev radiation, i.e., by division of the corresponding channels of the two halves.

The test sample (absorber) is pressed into circular Plexiglas disks of 11-mm internal diameter and 0.5–1.0-mm thickness and closed on both sides with sheets of plastic material, e.g., Sellotape. In investigating solutions or substances which are liquid at room temperature, similar containers are used with walls made of 30-μ thick aluminum foil. The liquid is filled into the container through a slit in the frame, which is sealed with cement.

The thickness of the absorber is chosen so that it contains 4–30 mg Fe per cm^2. Metallic absorbers are used with a thickness of 10–30 μ. In making measurements at various temperatures the absorber is in a thermally insulated airtight chamber which can be heated or cooled. The temperature of the chamber is measured with a thermoelement.

In addition to the usual determination of resonance in absorption it is possible, as Barloutaud (*1*) first showed, to carry out scattering experiments. Figures 10a and 10b show the velocity spectra of absorption and

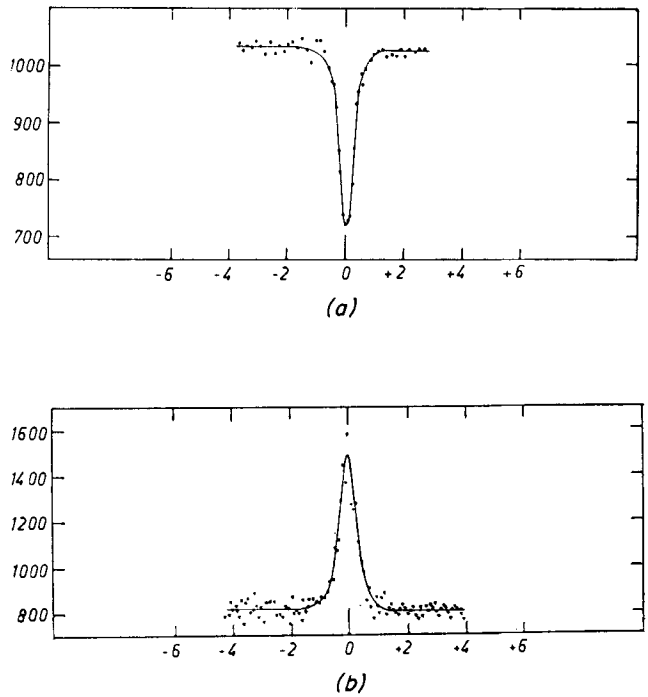

FIG. 10. Velocity spectrum of transmission and scattering measurements (*24*) with a Co^{57} source in Vacromium and (a) a Vacromium absorber, (b) a Vacromium scatterer. Ordinate: intensity of transmitted or scattered radiation (arbitrary units). Abscissa: relative velocity of source and absorber (mm/sec).

scattering measurements with a Co^{57} source in Vacromium G (stainless steel) and a Vacromium G absorber or scatterer. The scattering experiments allow, *inter alia*, the study of thick samples.

2. Radiation Sources

In studying the resonance of Fe^{57} nuclei, Co^{57} atoms which are incorporated into a crystal lattice are used as the source of radiation. The

Co^{57} atoms decompose according to the scheme shown in Fig. 7. Various authors have used sources in which Co^{57} is diffused into stainless steel, although approximately double the natural line width is obtained in this case. Approximately the same line width is also obtained with a Co^{57} source in copper. Particularly narrow emission lines are obtained by using platinum in place of stainless steel. The strong absorption of the radiation in the electron shell of platinum may be largely avoided by restricting the diffusion of the Co^{57} into it. The emission line from a source of Co^{57} in palladium is likewise narrow and only some 10% broader at the most than the natural line width. Absorption of the γ-radiation by palladium is also less than that by platinum. Figure 11 shows velocity spectra for $K_4[Fe(CN)_6]\cdot 3H_2O$ obtained with sources of Co^{57} in Pt, Pd, and Vacromium G (Fe, 55; Cr, 25; Ni, 20%).

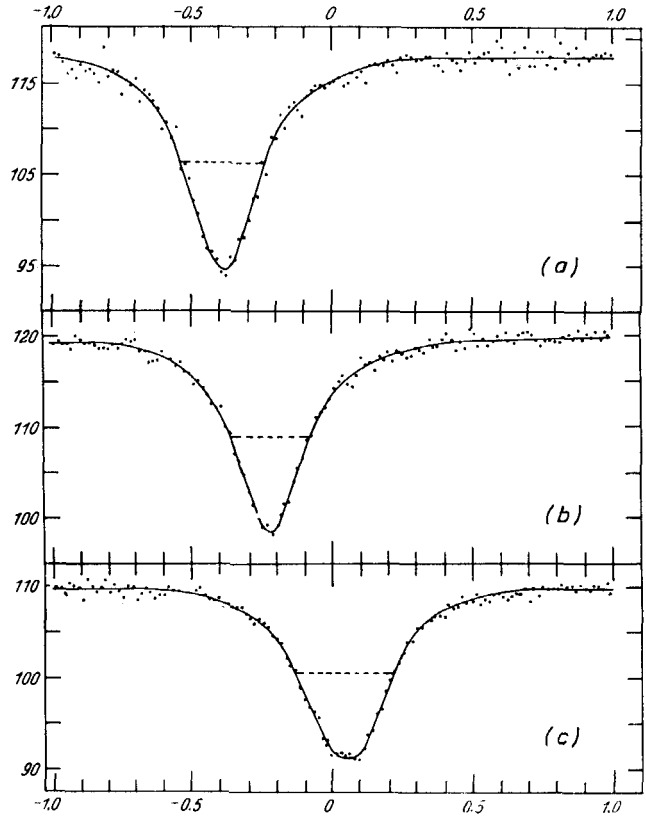

FIG. 11. Velocity spectrum of $K_4[Fe(CN)_6]\cdot 3H_2O$ with (a) Co^{57} in Pt, (b) Co^{57} in Pd, (c) Vacromium G. Ordinate: transmission (arbitrary units). Abscissa: relative velocity of source and absorber (mm/sec).

The line shift obtained with Co^{57} in palladium is 0.165 ± 0.002 mm/sec higher than that measured with Co^{57} in platinum, while the value found with Co^{57} in Vacromium G on the radiation source is shifted by 0.432 ± 0.002 mm/sec with respect to the value measured with Co^{57} in platinum. All the shifts recorded in this article refer to a source of Co^{57} in platinum unless otherwise mentioned. Table II gives the shifts δ for other metallic

TABLE II
VALUES OF THE SHIFTS δ FOR METALLIC SOURCES AND ABSORBERS[a]

Source: Co^{57} in	Shift (mm/sec) of	
	Source (+25°C)	Absorber (+25°C)
Vacromium G	0.432 ± 0.002	−0.431 ± 0.003
Fe	—	−0.351 ± 0.002
Cu	0.124 ± 0.010	−0.124 ± 0.011
Pd	0.165 ± 0.002	−0.165 ± 0.003
Pt	0	0.000 ± 0.002

[a] From Kerler *et al.* (*25*).

sources (25°) and the corresponding shifts δ for these systems as absorbers at 25°. The latter are given for Pt, Cu, and Pd sources and the possible differences between the source and the corresponding absorber have been taken into account in assessing the probable error.

3. Isomer Shift

The influence of the nature of the chemical bonding of the iron atom shows itself in the magnitude of the so-called isomer shift, in the temperature shift described in Section III,B,*4*, and in the quadrupole interaction which is discussed in Section III,B,*5*.

If the γ-radiation from a radiating source falls on an absorber which has nuclei bonded chemically in the same way and situated in the same crystal lattice as the source, then, from what has been said, resonance will occur. This is no longer the case if the nuclei in question in the resonance absorber are in a different state of chemical bonding from those in the radiation source. In order to satisfy the condition of resonance, it then becomes necessary to impart a definite velocity to the absorber relative to the source and thus change the energy of the incident quanta until they correspond to the excitation energy of the nuclei in the absorbing substance. The velocity may be positive or negative, i.e., in many cases the absorber must be moved towards the source and in others away from it, according to whether the excitation energy of the nucleus of the absorber is larger or

smaller than the energy of the γ-quanta emitted by the source of radiation. This shift relative to the zero velocity of an arbitrarily chosen radiation source is called the line shift.

It is made up of the isomer shift[3] and the temperature shift. The shift is usually expressed in terms of mm/sec or cm/sec. In order to convert data in Mc to cm/sec it is necessary to multiply by the conversion factor $h \times c/E$. E here represents the energy of the γ-quantum concerned. For the quanta from Fe^{57}, for example, 14,400 ev = 14,400 $\times$ 1.602 $\times$ 10^{-12} erg. The conversion factor for Fe^{57} is thus 8.643 $\times$ 10^{-3}.

The isomer shift describes the energy difference ΔE for the same energy transition in two atomic nuclei which have different electron wave functions at the nucleus. E is given by Eq. (15):

$$\Delta E = \frac{2Z \cdot e^2}{3} (R_B^2 - R_A^2) \{|\psi_a|^2 - |\psi_e|^2\} \tag{15}$$

where Ze is the nuclear charge, R_B and R_A are the nuclear radii of the excited and the ground state, respectively, and ψ_a and ψ_e are the wave functions at the nuclei in the absorber and emitter, respectively. The phenomenon was first observed by Kistner and Sunyar (*27*) for Fe^{57} and has since been found for Sn^{119} (*2*), Au^{197} (*48*), and other nuclei.

The isomer shift is a linear function of the s electron density at the nucleus and is caused by interaction of the s electrons with the different nuclear charge distributions in the excited state and ground state. [It may be noted that only the s electrons can have a finite density at the nucleus; p, d, and f electrons, which have zero density at the nucleus can nevertheless exert an influence on the electron density at the nucleus by screening the s electrons. Calculations on this screening effect for 3d electrons have been made by Watson and Freeman (*53*), and Walker *et al.* (*52*) applied these calculations to iron compounds.] The isomer shift decreases linearly with increasing s electron density at the nucleus, i.e., an increasing s electron density produces a shift of the resonance line to negative velocities. In the case of Fe^{57} the magnitude of the isomer shift is determined essentially by the occupation of the 3d and 4s states, and in certain cases by external effects (e.g., by the proportion of covalent-bonding or the fields of neighboring ions). This means, for example, that the shift for Fe^{2+} ions is more positive than that for Fe^{3+} ions because in the first case the 3s electrons are more strongly screened by the additional 3d electron (*8*, *49*, *52*).

[3] In the literature this quantity is also called the chemical shift. Since the latter term has come into use for the line shift occurring in nuclear magnetic resonance, the term isomer shift is preferred (isomeric nuclei are understood in nuclear physics to denote nuclei of equal charge and mass but different energy).

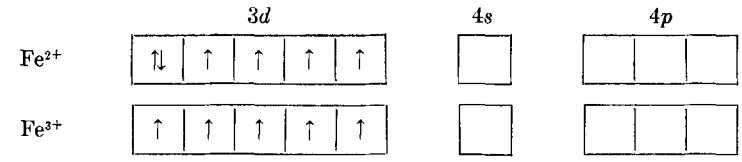

The high negative shift shown by metallic iron is a result of the high s electron density caused by the partial occupation of 4s orbitals.

Considering the values of the isomer shifts of numerous iron compounds given in Table III, it will be seen that these have characteristic values for

TABLE III

SHIFTS, QUADRUPOLE SPLITTINGS, AND THEIR TEMPERATURE DEPENDENCE FOR IRON COMPOUNDS

Absorber	Shift (at −130°C)	$-\Delta\delta/\Delta T$ (mm/sec/ 100°C)	Quadrupole splitting (at −130°C)	$-\Delta\epsilon/\Delta T$ (mm/sec/ 100°C)
$K_4[Fe(CN)_6]$	−0.333 ± 0.005	0.038	—	—
$(NH_4)_4[Fe(CN)_6]$	−0.360 ± 0.005	0.028	—	—
$Cu_2[Fe(CN)_6]$	−0.389 ± 0.006	0.036	—	—
$Ag_4[Fe(CN)_6]$	−0.397 ± 0.006	0.047	—	—
$K_3[Fe(CN)_6]$	−0.413 ± 0.003	0.039	0.373	0.06
$Cu_3[Fe(CN)_6]_2$	−0.454 ± 0.007	0.034	0.760	0.18
$Ag_3[Fe(CN)_6]$	−0.439 ± 0.007	0.035	0.860	0.06
$Na_2[Fe(CN)_5NO]$	−0.560 ± 0.003	0.030	1.725	
$Na_3[Fe(CN)_5NH_3]$	−0.284 ± 0.007	0.036	0.667	
$Na_4[Fe(CN)_5NO_2]$	−0.383 ± 0.007	0.038	0.855	
$Na_5[Fe(CN)_5SO_3]$	−0.322 ± 0.007	0.036	0.730	<0.01
FeS_2 (pyrite)	+0.033 ± 0.003	0.044	0.632	
FeS_2 (marcasite)	+0.007 ± 0.007	0.051	0.531	
$[Fe(dipyridyl)_3]Cl_2$	+0.039 ± 0.007	0.034	0.350	
$Fe(CO)_5$	−0.44 ± 0.003	0.05	2.532	—
$Fe(CO)_4I_2$	+0.08 ± 0.003	—	0.74	—
$Fe_2(CO)_9$	−0.192 ± 0.007	0.054	0.400	0.02
$Fe_3(CO)_{12}$ (outer lines)	−0.242 ± 0.010	—	1.098	0.10
$Fe_3(CO)_{12}$ (inner lines)	−0.302 ± 0.007	—	—	—
K_2FeO_4	−1.202 ± 0.005	0.041	—	—
$BeFeO_4 \cdot H_2O$	−1.195 ± 0.010	0.04	—	—
$BaFeO_4$	−1.159 ± 0.010	0.035	—	—
$KFeS_2$	−0.103 ± 0.010		0.504 (25°C)	—
$KFeO_2$	−0.116 ± 0.020	0.05	—	—
Red Roussin salt	−0.275 ± 0.007	0.040	0.667	0.03
Black Roussin salt	−0.216 ± 0.007	0.042	0.896	0.03
Fe^{2+} salts	+0.93 to +1.01	0.046–0.061	1.70–3.60	0.15–0.48
Fe^{3+} salts	+0.10 to +0.16	0.046–0.061	0–0.66	0–0.03
Fe metal	−0.264	0.056	—	—
Vacromium	−0.343	0.057	—	—

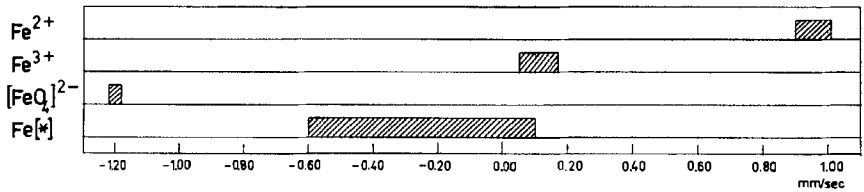

FIG. 12. Region of isomer shift for various classes of compound. Radiation source: Co^{57} in Pt at 25°. Abscissa: relative velocity of source and absorber (mm/sec).

various groups of iron compounds. Thus shifts for Fe^{2+} salts (Fig. 12) at about $-120°$ fall in the range 0.9–1.0 mm/sec, those for Fe^{3+} salts in the range 0.1–0.2 mm/sec [$FeCl_3 \cdot 6H_2O$ falls outside this range with $\delta = 0.555$ mm/sec (25°)], while complex compounds of iron vary between -0.6 and $+0.1$ mm/sec. Metallic iron itself ($\delta = -0.27$ mm/sec) falls in the last region. These ranges characteristic of the various states of bonding are discussed systematically in Section III,9.

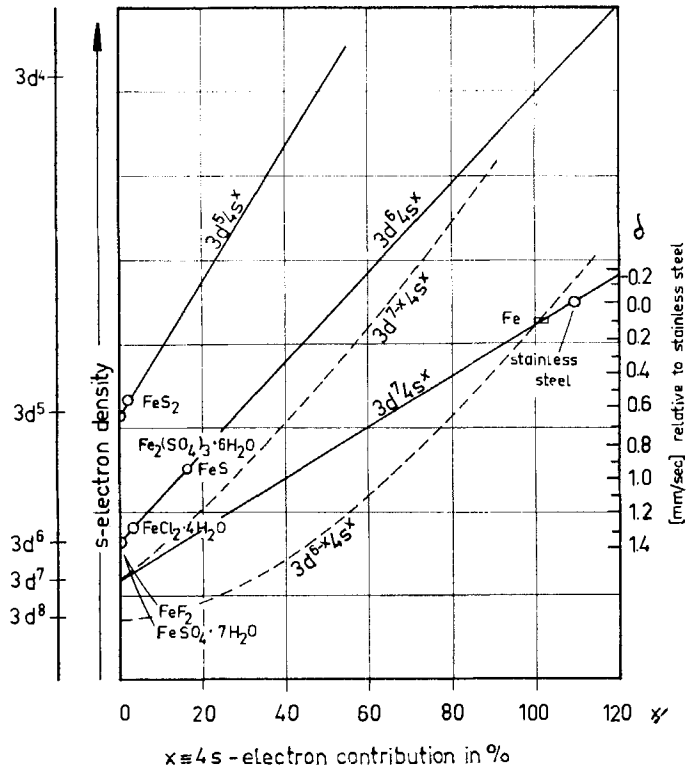

FIG. 13. Interpretation of the isomer shift. The total s electron density is represented as a function of the 4s character for various d electron configurations (*52*).

Walker and associates (*52*) combined the observed data, particularly for ionic compounds, with the Hartree-Fock calculations of Watson (*53*) on the various d configurations of iron in order to obtain a calibration of the isomer shifts in terms of the s electron density. The shift for iron in a transition metal alloy was explained by supposing that a certain proportion of a $4s$ electron is added to a $3d^7$ configuration of iron. This proportion could be determined by evaluating the $4s$ electron wave function density at the nucleus from the Fermi-Segrè-Goudsmit formula (*12*, *15*). Figure 13 shows this postulated relationship between the isomer shift and the total s electron density, which is expressed as a function of the percentage of $4s$ character for various d electron configurations. Shifts referred to stainless steel (type 310) are shown on the right-hand scale of the diagram. Shifts for ionic Fe^{2+} and Fe^{3+} compounds may be identified with Watson's densities for $3d^6$ and $3d^5$, respectively. The straight lines in the diagram represent s electron densities for hypothetical $3d^n4s^x$ configurations, while the dotted curves show the s electron densities for $3d^{8-x}4s^x$ and $3d^{7-x}4s^x$ configurations. Experimental values for some Fe^{2+} and Fe^{3+} compounds are shown on the $3d^64s^x$ or $3d^54s^x$ lines. It is readily seen that the $4s$ orbital of iron plays an increasingly important part as the ionic character of the bond diminishes: the electrons of the ligands occupy the $4s$ orbital in increasing measure. A high $4s$ electron density is observed in metallic iron and its alloys as one would expect. It does not depend much on the host metal, showing that the iron has essentially the same configuration in all cases.

4. Temperature Shift

In interpreting minor differences in shifts, it may be noted that the observed line shift is temperature dependent, i.e., is made up of the true isomer shift and a temperature shift. The proportion of the temperature shift in terms of the total line shift is generally small in relation to the isomer shift, being of the order of 0.05 mm/sec per 100°. The temperature dependence is practically linear in the region $-120°$ to $+80°$. Figure 14 shows shifts for a range of iron compounds as a function of temperature. Most salts show the same dependence on temperature as the metal, though complex salts give smaller values.

The temperature shift expresses both the magnitude of the Debye-Waller factor and the characteristics of the vibrational spectrum (*20*, *41*). It is proportional to the inner energy of the crystal, which reaches a saturation value with the excitation of all the lattice vibrations. The change of temperature shift with temperature is proportional to the specific heat.

The slope $-\partial\delta/\partial T$ depends only on the temperature shift if the s electron density is assumed to be independent of temperature. Whether the electron density arising from $3s$ and $4s$ electrons is actually independent

of temperature is undecided. In principle a temperature dependence seems possible if strongly dependent internal fields exist which can influence the electron distribution.

To compare δ values for various substances from the point of view of isomer shift, it is best to go to low temperatures where the temperature

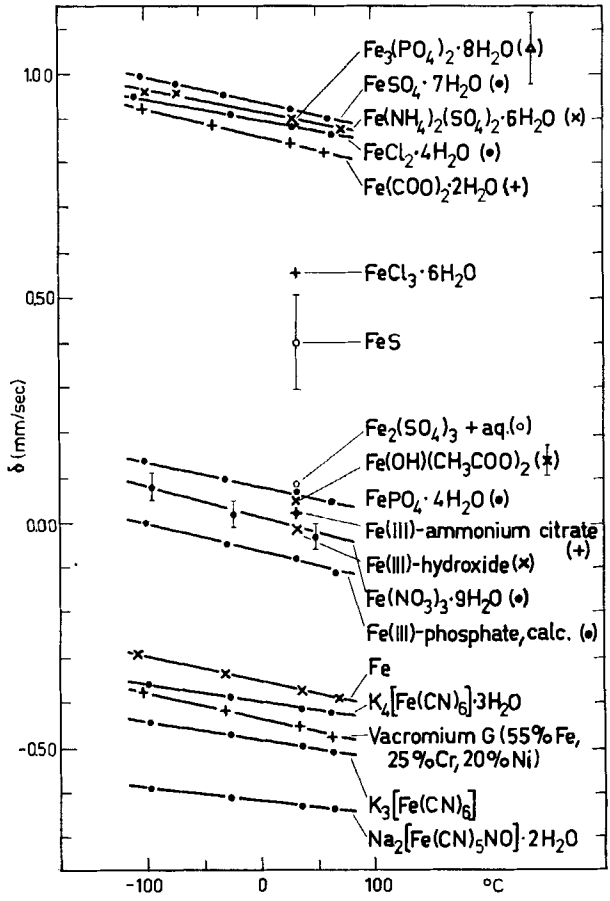

FIG. 14. Shift δ as a function of temperature. Ordinate: mm/sec. Abscissa: temperature (°C) (*23*).

shift is at a minimum. The differences in the contribution of the temperature shift are then substantially smaller and the residual mean contribution does not interfere with interpretation, provided comparisons are made with a source giving a definite shift.

In Table III the line shifts observed at low temperatures are specified.

The corresponding shifts at higher temperatures are tabulated in detail in the original publications (*13, 19, 24, 25, 26, 54*).

As has been said in the previous section, the observed shift depends on the nature of the radiation source. All the values given above refer to a Co^{57} source in platinum at 25°C. To convert the shifts from mm/sec to Mc it is necessary to multiply by 11.6 (cf. p. 452).

5. Quadrupole Splitting

In many cases it is found that the resonance line emitted from the substance examined consists not of one but of two lines, even when all of the nuclei in question are in the same state of bonding. The so-called quadrupole splitting of the resonance line arises from interaction of the electrical field gradient at the nucleus with the electrical quadrupole moment of the excited Fe^{57} nucleus. The field gradient at the nucleus depends on the electronic configuration of the atom in question and on its environment. [Good reviews of quadrupole interaction are given by Cohen and Reif (*5*) and by Das and Hahn (*7*).] Consequently conclusions may be drawn from the quadrupole splitting about the nature of the chemical bonding and the crystal lattice.

Quadrupole splitting of resonance lines was first studied by Kistner and Sunyar (*27*) with Fe^{57}. Here the position is particularly simple, since the ground state with a spin of $\frac{1}{2}$ has no quadrupole moment and splitting of the resonance line is due only to the excited state with a spin of $\frac{3}{2}$. Values for the quadrupole splitting ϵ (distances between the two lines) for the compounds studied are given in Table III. Figure 15 shows graphically

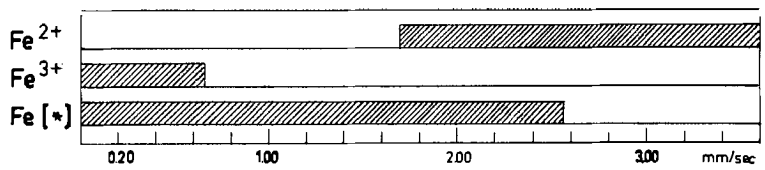

FIG. 15. Region of quadrupole splitting for various classes of compound. Abscissa: relative velocity between source and absorber (mm/sec) Fe[*] iron in complexes.

the quadrupole splitting characteristic of different types of compound, and Fig. 16 gives ϵ as a function of temperature for a series of compounds.

It is seen that Fe^{3+} salts have very small splittings up to about 0.6 mm/sec (*13, 24*) (see, for example, Fig. 17a). Unusually large splittings are observed in silicates containing iron (cf. Section III,B,*8,f*). They arise principally because of the field gradients produced by the crystal lattice at the nucleus, since the Fe^{3+} ion has a spherosymmetrical charge distribution and cannot give rise to any interaction with the electrical quadrupole

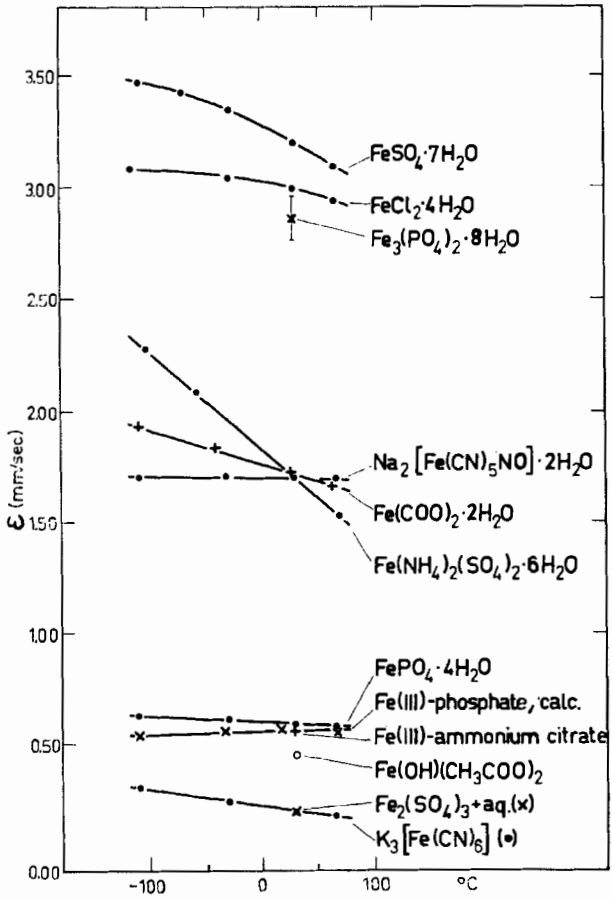

FIG. 16. Quadrupole splitting ϵ of absorption lines for various compounds as a function of temperature. Ordinate: mm/sec. Abscissa: temperature (°C) (*23*).

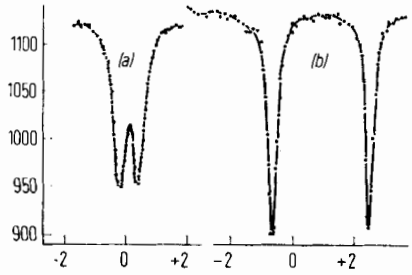

FIG. 17. Velocity spectra of (a) $FePO_4 \cdot 4H_2O$ and (b) $FeSO_4 \cdot 7H_2O$. Ordinate: transmission (arbitrary units). Abscissa: relative velocity of source and absorber (mm/sec).

moment. Field gradients in the crystal are strengthened by a factor of about 7 by Sternheimer antishielding (*50, 51*) of the Fe^{3+} shell, which is a polarization effect. An interpretation due to Burns (*4*) is satisfactory for explaining the relatively weak temperature dependence of quadrupole splitting for Fe^{3+} salts. This is attributed to the differential homogeneous contraction of the crystal in two axis directions.

The Fe^{2+} salts show very large quadrupole splittings due to the additional *d* electron (*8*). Depending on the temperature this electron occupies different terms split in the crystal field. This leads to a relatively large temperature-dependent field gradient at the nucleus. The velocity spectrum of $FeSO_4 \cdot 7H_2O$ is shown in Fig. 17b. Quadrupole splittings for Fe^{2+} ions generally fall in the range 1.7–3.6 mm/sec (*19*).

In the octahedral iron complexes which have been studied, two of the 3*d* orbitals of iron are used in forming the six hybrid orbitals and the 3*d* electrons are therefore accommodated in the remaining three 3*d* orbitals. These are fully occupied, for example, in a complex such as $[Fe(CN)_6]^{4-}$, leading to a spherosymmetrical charge distribution. Consequently $K_4[Fe(CN)_6] \cdot 3H_2O$ exhibits no quadrupole splitting. In the case of $K_3[Fe(CN)_6]$, where one electron is lacking to complete the filling of the remaining three 3*d* orbitals, splitting occurs, which, as in the case of Fe^{2+}, is strongly temperature dependent, (in place of an electron in addition to the half-filled shell in Fe^{2+} there is an electron hole in $[Fe(CN)_6]^{3-}$). For nitrosyl prussiates, on the other hand, one finds a large splitting which is practically independent of temperature, as would be expected for a complex ion with closed shells and this particular symmetry. The observed quadrupole splittings in iron complexes fall in the range 0–2.6 mm/sec.

6. Magnetic Splitting

Atomic nuclei often have a magnetic moment which may be considered as arising from a mechanical nuclear spin. The total angular momentum of such a nucleus is given by Eq. (16):

$$|\vec{I}| = \frac{h}{2\pi} \sqrt{[I(I+1)]} \tag{16}$$

where h is the Planck constant ($h = 6.624 \times 10^{-27}$ erg sec), and I is the nuclear spin number. From quantum mechanics the maximum observable component of the angular momentum is a whole or a half-integral multiple of $h/2\pi$:

$$\vec{I} = I\hbar \tag{17}$$

The nuclear spin I must be a multip'e of a half-integral or a whole number. The vectors of the magnetic moment of the atomic nucleus can have only

certain values in a magnetic field. The nuclear moment is able to take up $2I + 1$ orientations with respect to the field and the possible values are described by $2I + 1$ values of the magnetic quantum number m, namely

$$m = I, I - 1, I - 2, \cdots\cdots - (I - 2), -(I - 1), -I$$

Thus if the nuclear spin is $\frac{3}{2}$, for example, m may have the values $\frac{3}{2}$, $\frac{1}{2}$, $-\frac{1}{2}$, and $-\frac{3}{2}$. For nuclei with $I = \frac{1}{2}$, the possible values for m are $+\frac{1}{2}$ and $-\frac{1}{2}$. Each discrete value of the magnetic moment may couple with an external field or, as in our case, with the magnetic field produced at the nucleus by the crystal field and that due to the electron shell, so that the respective energy level will be split into a group of sublevels. In the case of Fe^{57} the excited state ($I = \frac{3}{2}$) splits into 4 energy levels and the ground state into 2 energy levels, as shown in Fig. 18. In accordance with the

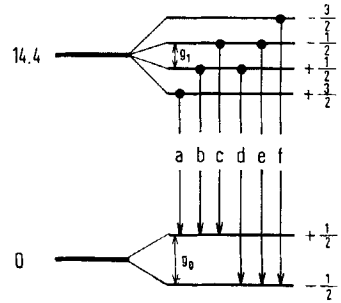

FIG. 18. Energy level scheme for the magnetic splitting of the ground state and the first excited state of Fe^{57} in metallic iron.

selection rule $\Delta m = 1,0,-1$, the six possible transitions between the levels of the excited state and the ground state give six resonance lines in the spectrum. Figure 19 shows the velocity spectrum of metallic iron. The

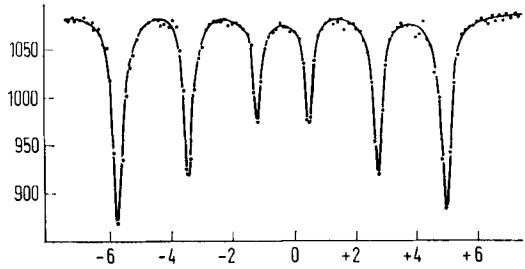

FIG. 19. Mössbauer spectrum of metallic iron at room temperature. Ordinate: transmission (arbitrary units). Abscissa: relative velocity between source and absorber (mm/sec).

splitting of the Fe^{57} ground state at 293°K is given by $g_0 = 3.924 \pm 0.008$ mm/sec, that for the excited state being 2.244 ± 0.005 mm/sec (*16*).

A detailed study of the Mössbauer spectrum of metallic iron was made by Hanna and associates (*16*, *44*). The six components of the spectrum persist to temperatures in the neighborhood of the Curie point of iron (769°). Even at 766.2° the six lines may be partially resolved, but at 768.4 they coalesce to a single broad structure. Above the Curie point only a single narrow line is observable (see also refs. *38*, *42*).

7. Line Width

Observed line widths are, from what was said in Section II, made up of the line width of the source and the absorber. The broadening produced by a finite thickness of absorber depends on $\sigma_0 \times n \times f'$, where σ_0 is the cross section for resonance absorption, n is the thickness of the absorber, and f' is the Debye-Waller factor for the absorbing substance. This broadening was determined with the aid of the diagram based on the calculations of Margulies and Ehrmann (*31*). In order to obtain better comparisons, this component, which generally amounts to 0.1–0.4 mm/sec,

TABLE IV
LINE WIDTHS Γ_0 FOR VARIOUS RESONANCE ABSORBERS

Absorber	Line width Γ_0 (mm/sec)
$FeSO_4 \cdot 7H_2O$	0.248 ± 0.008
$FeSO_4 \cdot (NH_4)_2SO_4 \cdot 6H_2O$	0.240 ± 0.008
$FeCl_2 \cdot 4H_2O$	0.257 ± 0.007
$Fe(COO)_2 \cdot 2H_2O$	0.230 ± 0.007
FeS (techn.)	0.9 ± 0.2
$FePO_4 \cdot 4H_2O$	0.441 ± 0.008
$Fe(NO_3)_3 \cdot 9H_2O$	1.2 ± 0.2
$FeNH_4(SO_4)_2 \cdot 12H_2O$	1.6 ± 0.2
$Fe_2(SO_4)_3 \cdot xH_2O$	0.33 ± 0.02
$FeCl_3 \cdot 6H_2O$	0.28 ± 0.02
$K_4[Fe(CN)_6] \cdot 3H_2O$	0.235 ± 0.005
$K_3[Fe(CN)_6]$	0.231 ± 0.005
$Na_2[Fe(CN)_5NO]2H_2O$	0.233 ± 0.005
Vacromium G (55% Fe, 25% Cr, 20% Ni)	0.387 ± 0.008
Fe (pure)	0.220 ± 0.006

is deducted from the measured values, thus eliminating the dependence on thickness and the temperature dependence arising from f'. Measurements with the same absorber at different thicknesses and temperatures are then in good agreement. A series of line widths Γ_0 obtained in this way are col-

lected in Table IV. It is seen that they are considerably greater in many cases than the value of $\Gamma_0 = 0.20$ mm/sec derived from the life of the 14.4-kev level of 1.0×10^{-7} sec. Disregarding very large values of the broadening ($\Gamma_0 = 0.35$ mm/sec), the approximate value of Γ_0 for Fe^{3+} salts is 0.31, for Fe^{2+} salts 0.24, for complex salts 0.23, and for metallic iron 0.22 mm/sec. The line broadening found by us (*13*, *24*, *25*, *26*) for the Co^{57} source in platinum is thus 10% at the most, i.e., the source has practically the natural line width.

Line broadening for various absorbers may be due to different causes: (1) the Fe^{57} atoms may not be uniformly incorporated in the crystal lattice, leading to a blurring of δ and ϵ; (2) very slow lattice vibrations may cause a change in the field gradient, which are not averaged as they are for higher frequencies; (3) magnetic interactions, even if these average up to zero; (4) with long spin correlation times the unresolved magnetic splittings give rise to a broad line.

8. *Examples of Applications*

The following sections describe the spectra of a number of iron compounds observed by us (*13*, *24*, *25*, *26*).

a. Berlin Blue. The problem of Berlin blue appeared to us to be of special interest as its structure and color have been the subject of a great deal of speculative discussion for many years.

"Insoluble Berlin blue" results when a solution of potassium hexacyanoferrate(II), $K_4[Fe(CN)_6]$, reacts with a solution containing Fe^{+++} ions in excess. It has the composition $Fe_4[Fe(CN)_6]_3$. The material is difficult to study chemically but with the aid of the Mössbauer effect it can be shown unambiguously that, contrary to earlier assumptions, well-defined oxidation states of +2 and +3 can be assigned to the iron atoms. They have discrete oxidation states rather than averaged values. Consequently the deep color of Berlin blue cannot be ascribed to fluctuating valencies or to resonance between structures such as

$$Fe^{II}(CN)_6Fe^{III} \leftrightarrow Fe^{III}(CN)_6Fe^{II}$$

Robin (*45*) recently came to the same conclusion from a study of the absorption spectrum of "soluble Berlin blue."

The Mössbauer spectrum of "insoluble Berlin blue" is shown in Fig. 20a. It is made up by superposing the dotted curves. Curve I shows the line characteristic of $[Fe(CN)_6]^{4-}$, while the spectrum consisting of Curves 2 and 3 represents a quadrupole splitting with the isomer shift characteristic of the Fe^{+++} ion. The ratio of intensities for the spectra 1 and (2 + 3),

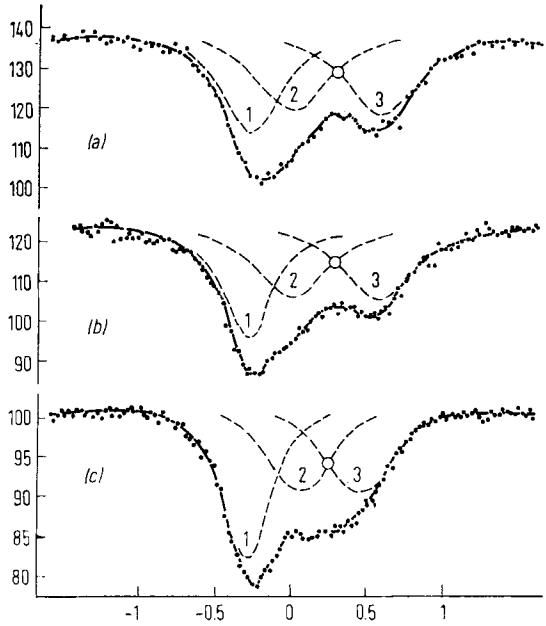

FIG. 20. Mössbauer spectrum of (a) insoluble Berlin blue,[4] (b) Turnbull's blue, and (c) "soluble Berlin blue" at −130°. Ordinate: transmission (arbitrary units). Abscissa: relative velocity of source and absorber (mm/sec).

within the accuracy of measurement, is 3:4, corresponding to the ratio of iron atoms in the oxidation states of +2 and +3.[4]

The spectrum shown in Fig. 20b is that of the so-called "Turnbull's blue," obtained by mixing a solution of potassium hexacyanoferrate(III) with excess of a Fe^{++} solution. It may be supposed that the first reaction taking place is

$$Fe^{++} + [Fe^{III}(CN)_6]^{3-} \rightarrow Fe^{+++} + [Fe^{II}(CN)_6]^{4-}$$

The reaction products then combine to form "insoluble Berlin blue."

When solutions of $K_4[Fe(CN)_6]$ and Fe^{+++} salts or $K_3[Fe(CN)_6]$ and Fe^{++} ions in a molar ratio of 1:1 are mixed, "soluble Berlin blue" of the composition $KFe[Fe(CN)_6]$ is produced in the colloidal form. The Möss-

[4] The method we have used in splitting up the spectrum into separate lines allows the energy to be determined exactly, but gives intensities with an accuracy of only about 30%. The ratio of intensities for the lines 1 and (2 + 3) does not correspond exactly to the required ratio 3:4. The mean of the intensity ratio obtained from many spectra of Berlin blue, however, was 0.72, which is near the theoretical value of 0.75.

bauer spectrum of "soluble Berlin blue" is shown in Fig. 20c. Line 1 corresponds to the hexacyanoferrate(II) ions, which are also present in this compound, while the doublet (lines 2 and 3) stems from Fe^{+++} ions. Intensities of 1 and (2 + 3) are in the ratio 1:1, corresponding to the ratio of Fe^{II} and Fe^{III} in the compound. It is thus a potassium iron(III) hexacyanoferrate(II). Assuming the structure for "soluble Berlin blue" proposed by Keggin and Miles (*22*), which is shown in Fig. 21; the results of our

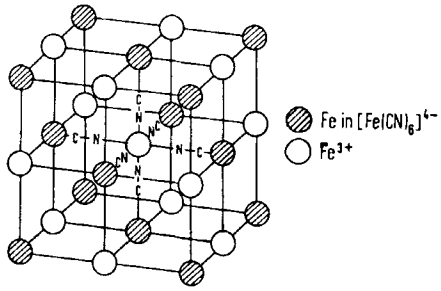

FIG. 21. Structure of "soluble Berlin blue." The potassium ions surround the central iron ion tetrahedrally (*22*).

investigation show that, if there are any bonds at all between iron and nitrogen, they can be only very weak and that iron in the 3+ state occurs essentially as an ion. In the light of these results an X-ray structural study of insoluble Berlin blue would be particularly interesting. Finally, susceptibility measurements are in agreement with our data. Soluble Berlin blue has a magnetic moment of 5.72 Bohr magnetons per molecule of $KFe[Fe(CN)_6]$, corresponding with five unpaired electrons per unit formula, as would be expected for a free Fe^{+++} ion.

It is notable in this connection that copper(II) and silver hexacyanoferrates(II), $Cu_2[Fe(CN)_6]$ and $Ag_4[Fe(CN)_6]$, show single unsplit resonance lines with almost the same isomer shift as the potassium salt or the lines due to $[Fe(CN)_6]^{4-}$ in $Fe_4[Fe(CN)_6]_3$. The copper(II) and silver hexacyanoferrates(III) give a Mössbauer spectrum with the strong temperature dependence characteristic of the $[Fe(CN)_6]^{3-}$ ion.

b. Prussiates. The prussiates are a group of compounds in which one cyano group of the hexacyanoferrate ion is replaced by another ligand as, for example, in sodium nitrosyl prussiate, $Na_2[Fe^{II}(CN)_5NO]$ or sodium ammino prussiate, $Na_3[Fe^{II}(CN)_5NH_3]$.

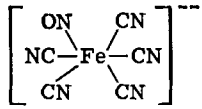

Nitrosyl prussiate ion

The Mössbauer spectrum of the first of these compounds is shown in Fig. 22. It consists of a doublet, the components of which are very widely split (ϵ = 1.723 mm/sec at room temperature). The quadrupole splitting proves to be practically temperature independent. Similar quadrupole splittings of various magnitudes are found for other prussiates. Isomer shifts for prussiates lie in the region which is characteristic of complex compounds. As is discussed fully later, their magnitudes are characteristic of the nature of the bond between the ligands and the central iron atom.

As was described in the previous section, $[Fe(CN)_6]^{4-}$ shows only a single unsplit resonance line. Because of the octahedral symmetry, the electrical field gradient and hence the quadrupole splitting is zero. The relationship is, however, different for prussiates, where the substituted ligands produce a different charge distribution, i.e., a finite field gradient is to be expected. This may have a positive or negative sign, according to the nature of the bond to the ligand in question.

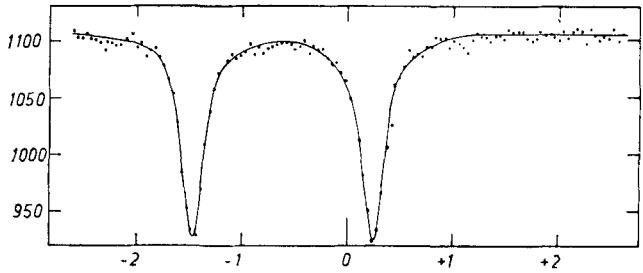

FIG. 22. Mössbauer spectrum of $Na_2[Fe(CN)_5NO]\cdot 3H_2O$. Ordinate: transmission (arbitrary units). Abscissa: relative velocity of source and absorber (mm/sec).

The cyano groups in hexacyanoferrate(II), $[Fe(CN)_6]^{4-}$, are linked to the central iron atom by σ-bonds. In addition each bond has a π-component which prevents the build-up of a high negative charge on iron ("back donation"). The bond relationships are illustrated in Fig. 23 and are valid

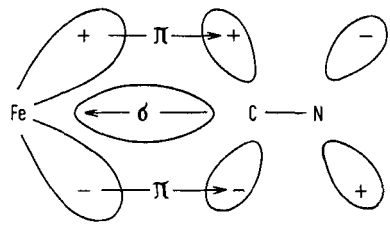

FIG. 23. Diagrammatic representation of bonding relationship between iron and a ligand with a Δ orbital.

in principle for all stable complexes. The π-bond removes charge from the central atom in accordance with the Pauling electroneutrality principle,

according to which the central atom can never have a charge greater than +1 or −1. As a result of the similar bond relationships occurring in all strong complexes, their isomer shifts all fall in a limited region situated in the position expected for Fe^0.

When the cyanide ligand in $[Fe(CN)_6]^{4-}$ is replaced by a ligand for which the π-bond has more weight, as in the example with NO^+, the electron density of the 3*d* orbital, from which the electrons for the π-bond are derived, is diminished. As a result, the line shift of the nitroprussiate ion relative to hexacyanoferrate(II) is negative. If the cyano group is replaced by NH_3 or NO_2^-, which are unable to form π-bonds, the reverse effect occurs: a shift in the direction of higher δ values relative to $[Fe(CN)_6]^{4-}$ is observed. Weak π-bonding is to be expected in the case of the sulfito complex $[Fe(CN)_5SO_3]^{5-}$, since only the diffuse *d* orbitals of sulfur are available for π-bonding. The observed isomer shifts of prussiates thus fall into the sequence

$$NO^+ > CN^- > SO_3^{--} > NO_2^- = NH_3$$

with increasing positive values of δ as the strength of the ligand π-bonding decreases.

No account has been taken of the σ-donor effect of the various ligands in what has been said above. This is permissible since a small change in the σ-donor component has little influence on the total *s* electron density involved, especially as a hybrid is involved in which the *s* electrons play a secondary part. In this connection attention may be drawn to another phenomenon, which is also observed in other cases. The dependence of the shift for the prussiate ion on the mode of bonding of the separate ligands shows that the three π-bonds present in the octahedral complex $[Fe(CN)_6]^{4-}$ are not divided among the remaining five cyano ligands if the sixth ligand is incapable of forming π-bonds. Instead the over-all π-bond component becomes smaller.

A π-bond of the separate ligand which is strong relative to CN^- leads to a positive field gradient, while for a weaker π-bond the field gradient is negative. It follows from what has been said above that only nitrosyl prussiate, $[Fe(CN)_5NO]^{--}$, among the compounds studied, has a positive field gradient: for all others a negative field gradient must be assumed.

c. Carbonyls. Three iron carbonyls are known, namely, the pentacarbonyl, $Fe(CO)_5$, the enneacarbonyl, $Fe_2(CO)_9$, and the dodecacarbonyl, $Fe_3(CO)_{12}$. The structures of the first two have been elucidated (*11*, *43*) and are reproduced in Figs. 24 and 25.

In iron pentacarbonyl the five CO groups are arranged at the corners of a trigonal bipyramid. The σ-bond system is based on a $d_{z^2}sp^3$ hybrid, while the eight electrons in the d_{xy}, d_{xz}, d_{yz}, and $d_{x^2-y^2}$ orbitals serve to form

the π-bonds from iron to the CO ligands. The π-bonds prevent the accumulation of a high negative charge on the iron atom in an analogous way to that described in subsection 6b.

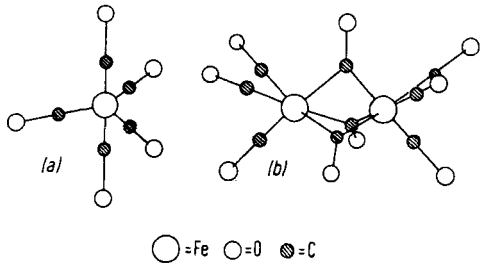

FIG. 24. Structure of iron pentacarbonyl (a).
FIG. 25. Structure of iron enneacarbonyl (b).

The trigonal bipyramidal arrangement of ligands leads to a finite electrical field gradient around the central iron atom which shows itself in the splitting of the iron resonance lines. The Mössbauer spectrum of $Fe(CO)_5$ is shown in Fig. 26. It consists of two lines, the separation of which corresponds to a quadrupole splitting of 2.53 mm/sec (−133°C).

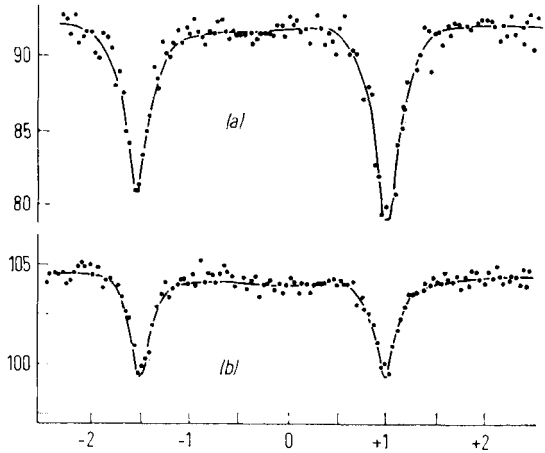

FIG. 26. Mössbauer spectrum of (a) undiluted $Fe(CO)_5$, (b) $Fe(CO)_5$ in tetrachloroethane. Ordinate: transmission (arbitrary unit). Abscissa: relative velocity of source and absorber (mm/sec).

The isomer shift amounts to -0.47 ± 0.08 mm/sec (−133°C). A notable feature of the spectrum of iron pentacarbonyl is that the left component of the doublet is smaller than the right. Kalvius *et al.* (*21*) showed by rotation of the sample that this arose from a preferred orientation of the

molecular field with respect to the direction of irradiation, and concluded that the field gradient and quadrupole moment were positive. Such a preferred orientation can occur readily in the crystallization of $Fe(CO)_5$, which is liquid above $-21°C$. Variation in the procedure may lead to different intensity relationships for the two lines. On the other hand we found that, using frozen solutions of $Fe(CO)_5$ in tetrachloroethane, the doublet consisted of two lines of equal intensity, showing that a homogeneous phase was present.

From the fact that frozen solutions may be used in studying the Mössbauer effect, two important possibilities for further application emerge: (1) isolated molecules or ions may be investigated independently of influences of the crystal lattice; (2) substances may be studied which cannot be isolated in the solid form or are stable only in solution.

In iron enneacarbonyl, $Fe_2(CO)_9$, each iron atom is approximately octahedrally surrounded so that it can be assumed that the σ-bonded system is made up of $d_{e_g}^2\ sp^3$ hybrids. Each of the terminal carbonyl groups contributes two electrons to the iron atom to which it is linked and each bridge CO group one, so that each iron atom has 17 electrons at its disposal, counting its own eight. Since the compound is diamagnetic the two "lone"

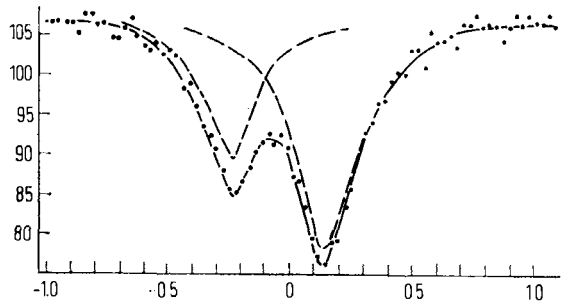

FIG. 27. Mössbauer spectrum of $Fe_2(CO)_9$. Ordinate: transmission (arbitrary units). Abscissa: relative velocity of source and absorber (mm/sec).

electrons must pair their spins in some way. The relatively short iron-iron distance found by crystal structure studies led to the supposition that there may be a covalent iron-iron bond. The results of our investigations are, however, in favor of a suggestion made by Orgel (*39*), according to which only a weak coupling of the unpaired electron spins suffices to explain diamagnetism of $Fe_2(CO)_9$. This could be brought about, for example, by the carbonyl bridges. The Mössbauer spectrum of iron enneacarbonyl is shown in Fig. 27. It exhibits a small quadrupole splitting as would be expected from the symmetrical environment of the iron atoms. The doublet

components are of different sizes and have an intensity relationship from which later discussion shows that the field gradient has a positive sign.

The structure of iron dodecacarbonyl, $Fe_3(CO)_{12}$, has so far not been elucidated. From infrared spectroscopy Mills (*32*) favored the second of the much discussed structures I and II which have been proposed. Dahl and Rundle (*6*), on the other hand, believe the assumption that the three iron atoms are arranged linearly, which has been supported by many authors, is incorrect. Dahl and Rundle prefer a structure in which the iron atoms are situated at the corners of a triangle.

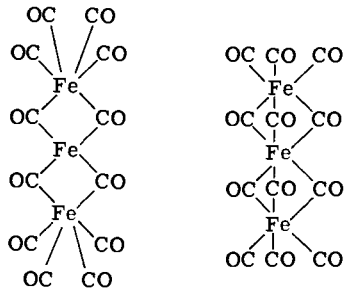

(I) (II)

The Mössbauer spectrum of the compound is reproduced in Fig. 28. It consists of three lines, the two outer of which correspond. The quadrupole splitting deduced from their separation is 1.09 mm/sec. The middle line is somewhat broadened relative to the other two, which may be due to a small

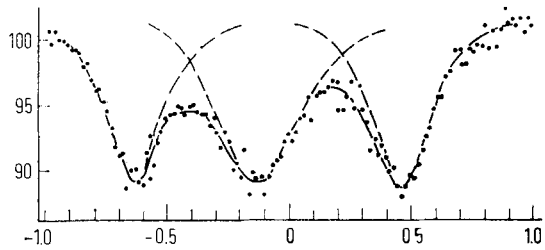

FIG. 28. Mössbauer spectrum of $Fe_3(CO)_{12}$. Ordinate: transmission (arbitrary units). Abscissa: relative velocity of source and absorber (mm/sec).

unresolved quadrupole splitting. The shape of the spectrum may be interpreted only on the basis of a structural model in which the iron atoms are in a line and the outer two are equivalent. Only the first of structures I and II can be reconciled without any difficulty with the results of our experiments and with the diamagnetism of the compound. In structure I the two outer iron atoms have an octahedral bond arrangement, while the middle

iron atom makes use of a tetrahedral d^3s hybrid. In accordance with this, one would expect the two outer iron atoms, four terminal CO ligands of which are opposite two bridging CO groups, to show a positive field gradient and splitting of the resonance line. On the other hand, the tetrahedrally surrounded central iron atom should give a single resonance line. This spectrum postulated for a molecule with structure I is in fact observed. The small broadening of the middle line can be understood readily as the result of a small distortion of the tetrahedral bonds. The electron configuration which has been described will also account for the diamagnetism.

In the hypothetical structure II, all three iron atoms would use d^2sp^3 hybrids for bonding so that the t_{2g} orbitals of each iron atom would remain occupied by four electrons. The somewhat different disturbance of the octahedral symmetry for the inner and outer iron atoms would lead to a different splitting of the corresponding $3d$ electron terms. This would explain the observation that there is a strong temperature-dependent quadrupole splitting for the outer iron atoms and a small one for the inner one. This electron configuration fails, however, to provide an explanation of the diamagnetism of the compound.

Figure 29 shows the Mössbauer spectrum of $Fe(CO)_4I_2$ in which, in contrast to $Fe(CO)_5$, the left line is stronger than the right. This again stems from the fact that the crystals are arranged with a preferred orientation, a phenomenon which can occur in powdered crystals and which is

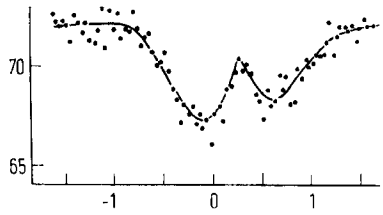

FIG. 29. Mössbauer spectrum of $Fe(CO)_4I_2$. Ordinate: transmission (arbitrary units). Abscissa: relative velocity of source and absorber (mm/sec).

often encountered in X-ray investigations. If the line in the spectrum belonging to the state $m = \pm\frac{3}{2}$ lies at more positive velocities than that belonging to the state $m = \pm\frac{1}{2}$, the field gradient is positive. If the reverse is true it is negative (see in this connection refs. *13*, *25*). A thorough investigation of the iron carbonyls and of $Fe(CO)_4I_2$ has also been made by Herber *et al.* (*18*).

d. Potassium Ferrate(VI) and Potassium Ferrate(III). Potassium ferrate(VI), K_2FeO_4, shows in its Mössbauer spectrum a very broad unsplit resonance line which is shifted to the left, with a δ value of about -1.20 mm/sec at $-120°C$. The absence of quadrupole splitting results from the

tetrahedral symmetry of the complex $[FeO_4]^{--}$ ion. It is possible to find, from the position of the absorption line and the lack of splitting, which of the two possible bond hybrids directed towards the corners of the tetrahedron is used for the σ-bond system. According to Watson's calculation (*53*) for an sp^3 hybrid, a δ value would be expected which lies substantially lower than that measured. The $3d$ orbitals of iron would then be occupied by only two electrons, so that the screening action on the s electron density would be very small. Wertheim and Herber came to the same conclusion (*55*). In addition a temperature-dependent splitting should be observed with sp^3 hybridization.

In potassium ferrate(III) each iron atom is surrounded tetrahedrally by four oxygen atoms. The tetrahedra are linked at their edges. The δ value of potassium ferrate(III) is only about 0.22 mm/sec more negative than $\delta_{Fe^{+++}}$, i.e., the s electron density in the ferrate(III) is not much greater than in the free Fe^{+++} ion. The small shift is caused by the small contribution which the sp^3 hybrid makes to the s electron density, for the bonds between oxygen and iron are purely σ in character. That the contribution of the sp^3 hybrid is so small is probably related, *inter alia*, to the fact that a hybridized $4s$ electron increases the s electron density less than a normal $4s$ electron and that the bonds are also already strongly heteropolar.

e. Potassium Dithioferrate(III). In potassium dithioferrate(III), $KFeS_2$, the $[FeS_2]^-$ ions are arranged in chains of FeS_4 tetrahedra linked by their edges. As in the case of $KFeO_2$, the chains may be considered as multicenter ions. While $KFeO_2$ shows magnetic splitting up to at least several hundred degrees, this occurs for $KFeS_2$ only at low temperatures. Figure 30a shows the spectrum of $KFeS_2$ with a pure quadrupole splitting at 25°, while in Fig. 30b there is an additional magnetic splitting at −145°. The spectra with pure quadrupole splitting may be interpreted in the usual way, but it should be noted that, in the case of magnetic splitting, the electrical quadrupole splitting must also be taken into account.

Compared with a spectrum showing pure magnetic interaction, the four inner lines in the figure are somewhat shifted to the right and the two outer lines are shifted to the left, so that the spacing of the outer lines to the right and left are no longer equal. The intensities of the lines relative to one another are those which would be expected for magnetic splitting with a finite thickness of absorber. This is in agreement with the observed position of the lines. Figure 31a shows schematically how the spectrum in Fig. 30b arises: the magnetic interaction first leads to splittings of the ground state and the first excited state of Fe^{57} characterized by g_0 and g_1; these combine to give the structure shown in Fig. 31b, taking into account the approximate ratio of the magnitudes of the magnetic moments. The substates of the excited state with $m = \pm\frac{3}{2}$ are then displaced to lower values and that with

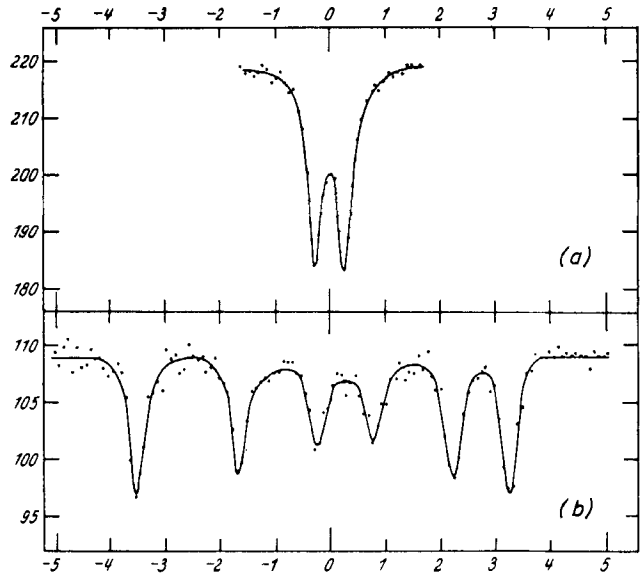

FIG. 30. Mössbauer spectrum of $KFeS_2$: (a) at 25°, and (b) at −145°. Ordinate: transmission (arbitrary units). Abscissa: relative velocity of source and absorber (mm/sec).

$m = \pm\frac{1}{2}$ raised by the electrical quadrupole interaction. The six possible transitions are indicated in the spectrum. If the asymmetry parameter of the field gradient $\eta = (V_{xx} - V_{yy})/V_{zz}$ (see p. 480) disappears and the direction of the magnetic field coincides with the main axis of the field gradient, the shifts of the excited substates (Fig. 31a) are exactly $\epsilon/2$ (as

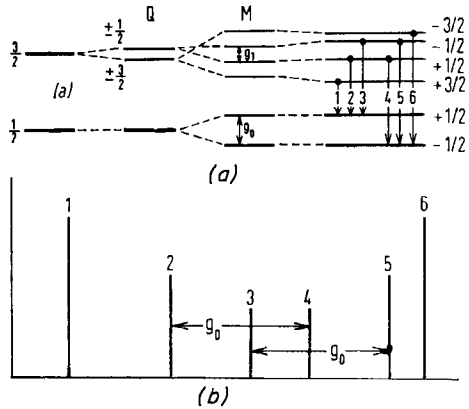

FIG. 31. (a) Energy level scheme for the superposition of quadrupole splitting and magnetic splitting. (b) Spectrum to a first approximation.

they are without a magnetic field, when they lead to a quadrupole splitting of ϵ), and a lowering of the excited substates with $m = \pm\frac{3}{2}$ and a raising of those with $m = \pm\frac{1}{2}$ correspond to a negative field gradient. In the general case, these shifts are neither equal in amount nor can conclusions be drawn from them directly about the sign of the field gradients.

The interpretation of spectra such as that in Fig. 30b may be made on the basis of the scheme shown in Fig. 31a: g_0 is obtained as the distance between the lines 2 and 4 or 3 and 5; δ is obtained as the mean value of the positions of lines 1, 2, 5, and 6 or 1, 3, 4, and 6 since the sum of the energies of interaction E_n for the four excited substates must be zero in this case: E_n is obtained similarly from the positions of the corresponding lines. Since only three of the four E_n values are independent because of the condition $\Sigma E_n = 0$, the five quantities, g_1, ϵ, η, θ, and φ may now be determined if two of them can be evaluated in another way (θ and φ are polar and azimuthal angles of the magnetic field in the coordinate system of the field gradient).

The magnetic field at the nucleus is obtained from g_0 and the magnetic moment of the ground state of Fe^{57}. Since our standardization of velocities is based on the value $g_0 = 3.96$ mm/sec for metallic iron at 25°, and this corresponds to a field at the nucleus of 333 kilogauss, the measured values of g_0 must be multiplied by a factor of 84.09 kilogauss/mm/sec in order to obtain the magnetic field at the nucleus. For $KFeS_2$ the magnetic field at the nucleus decreases from 206 kilogauss at −145° to zero at −28°, but for $KFeO_2$ from 515 kilogauss at −123° only to 490 kilogauss at 75°. This shows the existence of a high transition point for the latter compound.

Figure 32 shows δ for $KFeS_2$ as a function of temperature. Near the transition point there is a deviation from the otherwise normal and approximately linear relationship. If the isomer shift is assumed to be inde-

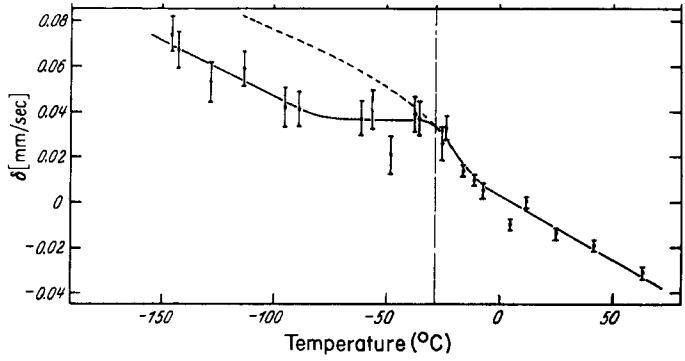

FIG. 32. Shift δ in the spectrum of $KFeS_2$ as a function of temperature. Ordinate: shift (mm/sec). Abscissa: temperature (°C).

pendent of temperature, $-\partial\delta/\partial T$ is proportional to the specific heat. This is known to have a maximum at the Curie or Neel point, which the dotted curve leads one to expect. The deviation below the transition point may be explained by a temperature-dependent component of the isomer shift which is approximately proportional to the magnetic field.

f. Silicates Containing Iron. A number of typical silicates containing iron have been studied by De Coster, Pollak, and Amelinckx (*9*, *40*). The Mössbauer absorption spectra were obtained, unless otherwise noted, with powdered silicate samples and are shown in Figs. 33–35. The isomer shifts given in this section refer to Co^{57} in Cr. The half width Γ of stainless steel as absorber was 0.48 mm/sec for the source used.

Epidote, $Ca_2(Al,Fe^{3+})_3[OH(SiO_4)_2]$, contains only one sort of Fe(III) ions, which are surrounded by O^{2-} ions. Accordingly the spectrum shows only a doublet, the center of which shows an isomer shift of 0.53 mm/sec[5] characteristic of Fe^{3+} ions. The quadrupole splitting observed was $\epsilon = 2.07$ mm/sec. This large splitting was caused by a strong electrical field gradient resulting from the anisotropic environment. An even larger splitting for Fe^{3+} ions was observed earlier by Shirane *et al.* (*47*) for Fe_2TiO_5 ($\epsilon = 3.5$ mm/sec).

Augite, which may be described as a mixture of layers of acmite, $NaFe(SiO_3)_2$, and diopside, $CaMg(SiO_3)_2$, layers, contains SiO_4 tetrahedra joined by two oxygen bridges into chains. Iron in acmite is tervalent while that which partially replaces magnesium in the diopside layers is bivalent. A quadrupole splitting would be expected for both resonance lines because of the unsymmetrical environment. The spectrum of augite is reproduced in Fig. 33. It can be resolved readily into two doublets (dotted curves), the strongest of which shows an isomer shift of 1.37 mm/sec characteristic of Fe^{2+} ions while that for the second (0.54 mm/sec) is typical of the Fe^{3+} ion. The measured value of the quadrupole splittings of the first and second doublets are 2.18 and 1.08 mm/sec, respectively.

Tourmaline, which may be represented by the formula $(Na,Ca)(Mg,Li,Fe,Al)_3(Al,Fe,Mg)_6[(OH)_4(BO_3)_3Si_6O_{18}]$ is, like augite, a silicate with Si:O = 1:3. The oxygen tetrahedra which surround each silicon atom are linked by two corners and form closed rings rather than infinite chains. The relatively complex structure of the spectrum reproduced in Fig. 34 shows at once that the iron in this mineral is present in various states and environments. The authors have resolved the spectrum into three doublets. The first two bands are due to Fe^{2+} ions ($\delta = 1.15$ mm/sec or 1.40 mm/sec; $\epsilon = 2.10$ mm/sec or 2.61 mm/sec). Since the isomer shifts are different for the two Fe^{2+} ions, the authors discussed the result in terms of different

[5] The shifts for the Co^{57} source in chromium used by the authors were about 0.4 mm/sec higher than for a source of Co^{57} in platinum.

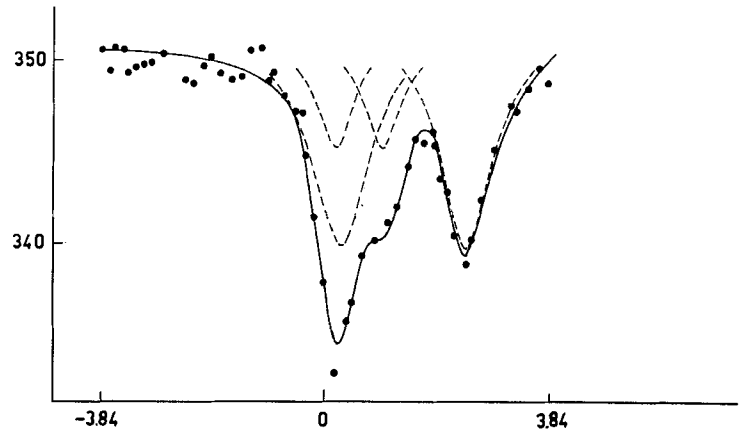

FIG. 33. Mössbauer spectrum of augite. Radiation source Co^{57} in Cr (*9*). Ordinate: transmission (arbitrary units). Abscissa: relative velocity of source and absorber (mm/sec).

configurations relative to the OH groups, i.e., to the different positions of the protons. The protons influence the $\pm\frac{1}{2}$ levels but not the $\pm\frac{3}{2}$ levels. The difference in interaction energy between protons and the $\pm\frac{1}{2}$ state is 0.51 $\pm$

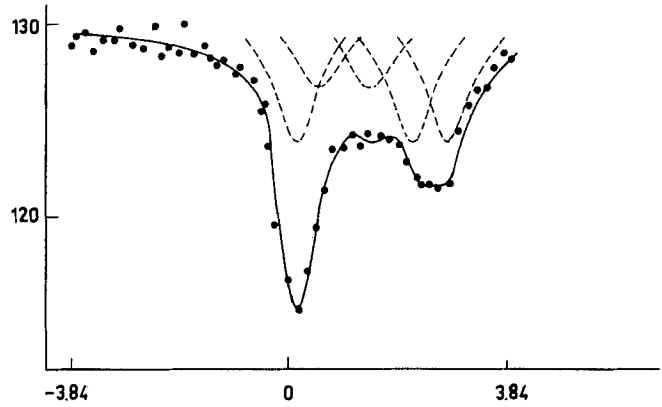

FIG. 34. Mössbauer spectrum of tourmaline. Radiation source Co^{57} in Cr (*9*). Ordinate: transmission (arbitrary units). Abscissa: relative velocity of source and absorber (mm/sec).

0.07 mm/sec = 5.8 $\pm$ 0.8 Mc/sec. The third doublet is attributed to the presence of Fe^{3+} ions, although the observed isomer shift of 0.95 mm/sec is very high. The quadrupole splitting was 0.91 mm/sec.

Biotite is a micaceous mineral. The sequence of layers is of the type (*10*):

. . . [O—Si—(O—OH)—R—(O—OH)—Si—O—X] . . .

The lattice position R may be occupied by Mg^{++}, Al^{+++}, Fe^{++}, Li^{+}, and Mn^{++}, while the X positions may be occupied by Na^{+} or K^{+} (*56*). Silicon may be partially replaced by aluminum, the missing positive charge being compensated for by replacement of a bivalent ion in the R layer by a tervalent iron ion. The structure of biotite described by Wyckoff (*57*) contains iron in two different environments, which may be described as distorted octahedra.

Figure 35 shows the Mössbauer spectrum of a single crystal of biotite. It consists of two bands A and B, the first of which is sharper than the second. This excludes the possibility that we are dealing with the quadrupole splitting of a single line. Rather, it supports the assumption that there are two different types of iron atom, each of which gives rise to a

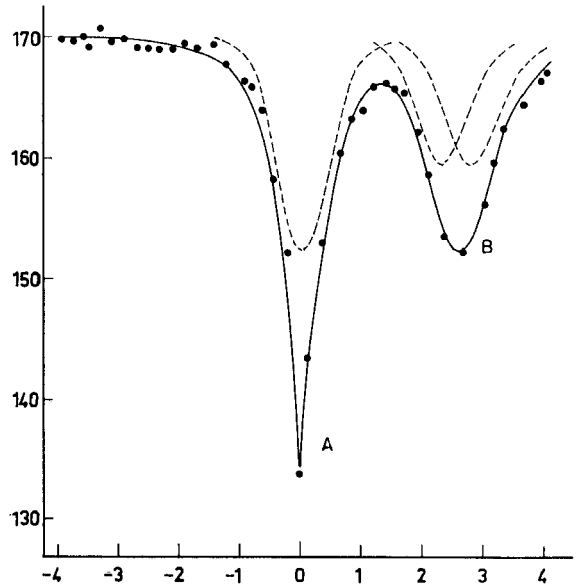

FIG. 35. Mössbauer spectrum of biotite. Radiation source Co^{57} in Cr (*40*). Ordinate: transmission (arbitrary units). Abscissa: relative velocity of source and absorber (mm/sec).

doublet. The centers of the doublets fall in the region characteristic of Fe^{++} ions. Resolution of the spectrum into two doublets is shown by the dotted curves in Fig. 35. The components of each doublet on the left almost coincide and are separated by 0.05 mm/sec at the most. They produce the resonance band A (δ = 0.022 mm/sec). The components of the two doublets on the right lie at 2.43 and 2.83 mm/sec. The isomer shifts for the two

types of iron are 1.23 and 1.42 mm/sec, the quadrupole splittings being 2.41 and 2.81 mm/sec.

Staurolite, olivine, and actinolite give spectra which consist of a doublet. Olivine, $(Mg,Fe)_2(SiO_4)$, belongs to the structures with discrete anions. The tetrahedra in $Ca_2Mg_{2-5}Fe_{0-3}[OHSi_4O_{11}]_2$ form bands, and staurolite may be described as cyanite, $Al_2O[SiO_4]$, into which $Fe(OH)_2$ layers are built. In all these cases bivalent iron is in an octahedral environment and accordingly gives rise to a spectrum which is split into a doublet. The isomer shifts and quadrupole splittings are shown in Table V.

TABLE V
ISOMER SHIFT, QUADRUPOLE SPLITTING, AND LINE WIDTHS OF SOME SILICATES (SOURCE Co^{57} IN Cr)

Silicate	δ (mm/sec)	ϵ (mm/sec)	Γ (mm/sec)
Staurolite	1.14	2.22	0.88 ± 0.05
Olivine	1.35	3.04	0.70 ± 0.04
Actinolite	1.32	2.41	1.06 ± 0.09

Bronzite, $(Mg,Fe)_2Si_2O_6$, also contains Fe^{++} ions and again gives a spectrum consisting of a doublet. The intensities of the two components of the doublet are somewhat different, an observation which has been made in other cases (e.g., for $Fe(CO)_5$: see p. 467): it may be attributed to a preferred orientation of the bronzite crystallites.

g. Iron π-Complexes. Ferrocene or dicyclopentadienyl iron, $Fe(C_5H_5)_2$, a "sandwich" compound, in which the iron atom lies between two five-membered aromatic hydrocarbon rings (Fig. 36) and ferricinium salts, e.g.

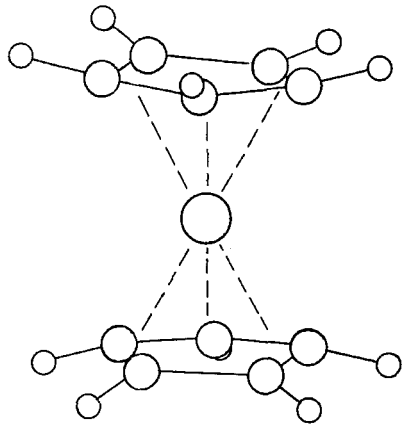

FIG. 36. Structure of ferrocene $Fe(C_5H_5)_2$.

$[Fe(C_5H_5)_2]Br$, have been investigated by Wertheim and Herber (*55*). Both compounds display approximately the same isomer shift, equal to 0.65 mm/sec (295°K) or 0.52 mm/sec relative to a Co^{57} source measured in stainless steel. The quadrupole splittings of the two compounds, on the other hand, are very different: ϵ for ferrocene at 20°K is 2.3 mm/sec, whereas the ferricinium ion exhibits only a small quadrupole splitting of about 0.2 mm/sec, which shows itself as a broadening of the line. In spite of the fact that strong screening of the *s* electrons by the ten 3*d* electrons is to be expected in ferrocene, the observed isomer shift is relatively small. In order to account for this low value, Herber *et al.* suggested that the 4*s* electrons participate to the extent of about 30% in the bonding. Another explanation would be the formation of π-bonds from iron to the cyclopentadienyl rings (back donation), which would involve electrons of the d_{yz} and d_{xz} orbitals. The very small quadrupole splitting in ferricinium salts is, according to Zahn *et al.* (*58*), due to a fortuitous compensation of the large electrical field gradients of the σ and π orbitals, on the one hand, and of the δ orbitals, on the other.

Study of a series of ferrocene derivatives shows that the bonding of the iron atom is virtually unaffected by ring substitution. Neither the isomer shift nor the quadrupole splitting changes appreciably on such substitution (*55*).

The small isomer shift in the cyclooctatetrene complexes $(C_8H_8)Fe_2(CO)_3$ and $(C_8H_8)[Fe(CO)_3]_2$ is also indicative of a well-developed π-bond system. The shifts, which were measured at 78°K, and were referred to Co^{57} in chromium, amounted to 2.3 ± 0.1 mm/sec and 1.8 ± 0.1 mm/sec. The almost equal shifts show that the environment of the iron atoms must be very similar in the two compounds. In keeping with this assumption, the line widths in the two compounds are found to be approximately the same (0.32 and 0.33 mm/sec). All observations support the conclusion made from NMR and infrared studies that the C_8H_8 rings in both compounds are planar. Table VI gives the quadrupole splittings of some iron π-complexes with cyclooctatetrene as ligand.

TABLE VI
QUADRUPOLE SPLITTINGS IN IRON π-COMPLEXES

Complex	ϵ (mm/sec)
$(C_8H_8)Fe(CO)_3$	1.23
$(C_8H_8)[Fe(CO)_3]_2$	1.32
$(C_8H_8)_2Fe(CO)_3$	1.60
$(C_8H_8)[C_2(CN)_4]Fe(CO)_3$	0.86

h. Miscellaneous Compounds. α-Dipyridyl reacts readily with iron(II) chloride to form the complex $[Fe(dipyr)_3]Cl_2$, the bonding being quite similar to that in hexacyanoferrate(II). The σ-bond system is a d^2sp^3 hybrid and a transfer of charge from the iron atom to the ligands is made possible by delocalized $p\pi$ orbitals. The Mössbauer spectrum of the compound shows a small quadrupole splitting which is practically temperature independent, confirming that the octahedral symmetry is somewhat distorted by the bifunctional ligands.

The spectrum of pyrites and marcasite, the disulfides of iron, FeS_2, shows a similar largely temperature-independent quadrupole splitting. The shift for the two compounds shows that, in agreement with Klemm's magnetic measurements, iron is in the +2 oxidation state and not in the +4. The shift also falls in the range which is characteristic of complex compounds. In these two compounds, iron uses what are essentially d^2sp^3 hybrids for its bonding, the bonds having extensive covalent character. Pyrite has a rock salt lattice with dumbbells formed by two sulfur atoms (S—S = 2.14 Å) situated with their mass centers at the sites of the chloride ions. The iron atoms are then in an environment which is not strictly octahedral and this is responsible for the small quadrupole splitting.

i. Chemistry of Surfaces. Brady *et al.* (*3*) have opened up this interesting range of applications of Mössbauer spectroscopy. All the experiments described so far were directed towards the study of the chemistry of the absorber but, in certain problems, it is better to vary the radiation source in a suitable way. A carrier-free solution of Co^{57}/Fe^{57} is added to the supernatant solution from which Fe(II) oxalate has been precipitated and the precipitate is filtered after some time. The Mössbauer spectrum of the radiation emitted by the material adsorbed on the surface of the precipitate is then studied, using an absorber consisting of nonmagnetic stainless steel. It is found that there is the same isomer shift and the same quadrupole splitting as in the spectrum of a Co^{57} source (on copper) with an iron(II) oxalate absorber. It is found that more than 40% of the Fe^{57} atoms adsorbed onto the surface occupy lattice sites corresponding to those in crystalline inactive iron(II) oxalate. Clearly extensive recrystallization has occurred or there has been exchange with layers of atoms below the solid surface. Analogous investigations, in which a cobalt(II) oxalate precipitate was used, led to similar results.

9. *General Interpretation of Various Effects in the Mössbauer Spectroscopy of Fe^{57}*

a. Temperature Shift. Temperature shifts, $-\partial\delta/\partial T$, for complex salts lie between 0.03 and 0.04 (mm/sec)/100° but otherwise are in the range 0.05–0.06 (mm/sec)/100°. With the aid of $-\partial\delta/\partial T$, the contributions of

the temperature shift to the total line shifts at low temperatures ($-130°$) and their differences for individual compounds may be estimated. This is needed in the discussion of finer differences. The specific heat decreases regularly with decreasing temperature, apart from the behavior at transition points (Curie point, etc.). The value of δ less the temperature shift of the absorber consequently lies between the values at $-130°$ given in Table III and the values extrapolated to $-273°$, i.e., the contribution of the temperature shift to δ at $-130°$ between 0 and $143 \times \partial\delta/\partial T$. The mean value for complex salts is -0.025 (mm/sec)/100° and for other compounds it is -0.04 (mm/sec)/100°, while differences within the two groups are of the order of 0.01 (mm/sec)/100°.

b. Influence of the Crystal Lattice. As may be seen from Table III, the value of δ changes little if ions such as Fe^{2+}, Fe^{3+}, $[Fe^{II}(CN)_6]^{4-}$, $[Fe^{III}(CN)_6]^{3-}$, or $[Fe^{VI}O_4]^{2-}$ are incorporated in different crystal lattices. The same is true for molecules such as $Fe(CO)_5$, as may be seen from measurements on frozen solutions. The value of δ is thus primarily characteristic of the isomer shift of the particular iron ion or molecule. Influences of the crystal lattice on the isomer shift, as in the case of the temperature shift, must be examined in the light of more exact studies of the isomer shift. Valuable conclusions can then be drawn from small differences. Thus, for example, the value of δ for Fe^{2+} and Fe^{3+} salts changes by about 0.08 mm/sec, and for $[Fe^{II}(CN)_6]^{4-}$ in the form of K^+, NH_4^+, Cu^{2+}, and Ag^+ salts by about 0.06 mm/sec. These differences can no longer be explained by the temperature shift, but clearly depend for the most part on differences in the isomer shift. They may be explained by the fact that the ionic character in the copper and silver salts is reduced and that a small covalent component enters into the bonding. Occupation of the $3d$ orbitals is reduced as a result of this covalent component, and as a result the $3s$ electron density at the site of the nucleus is increased because of reduced screening. Differences which occur in the isomer shift of Fe^{2+} and Fe^{3+} salts may be explained similarly, the small value of δ for $FeSO_4 \cdot 7H_2O$ in relation to that for $Fe(COO)_2 \cdot 2H_2O$ being particularly striking.

c. Quadrupole Splitting. The quadrupole splitting, ϵ, which arises from the interaction of the electrical field gradient with the quadrupole of the excited Fe^{57} nucleus, is proportional to

$$\frac{\partial^2 V}{\partial z^2}\sqrt{1+\eta^2/3}$$

where

$$\eta = \left(\frac{\partial^2 V}{\partial x^2} - \frac{\partial^2 V}{\partial y^2}\right) \Big/ \frac{\partial^2 V}{\partial z^2}$$

the asymmetry parameter, and $\partial^2V/\partial x^2$, $\partial^2V/\partial y^2$, and $\partial^2V/\partial z^2$ (abbreviated V_{xx}, V_{yy}, and V_{zz}) are the components of the field gradient. The coordinate system may in addition be chosen so that

$$|V_{zz}| \geqq |V_{yy}| \geqq |V_{xx}|$$

We then have

$$-1 \leqq \eta \leqq +1$$

and

$$1 \leqq \sqrt{1 + \eta^2/3} \leqq 1.16$$

The quantity ϵ is approximately proportional to $\partial^2V/\partial z^2$. With the aid of ϵ and $\Delta\epsilon/\Delta T$ in columns 4 and 5 of Table III, it is possible to obtain an over-all picture of how the electrical field gradient varies in different compounds. The values, which have been rounded, have been determined for ϵ at $-130°$ and for $\Delta\epsilon/\Delta T$ in the range $-130°$ to $+25°$. The mean slope $\Delta\epsilon/\Delta T$ has been used in place of $\partial\epsilon/\partial T$ because deviations from linearity are observed for some compounds, i.e., $\partial\epsilon/\partial T$ decreases with decreasing temperature in the case, for example, of some Fe^{2+} salts.

The values of ϵ for the compounds investigated in the ranges shown appear in Fig. 16. Considering the temperature dependence of the quadrupole splitting (Fig. 16) it will be noted that for Fe^{2+} salts and $[Fe(CN)_6]^{3-}$ it is relatively large, with values of $-\Delta\epsilon/\Delta T = 0.06$–$0.43$, whereas iron in an oxidation state of $+2$ in complexes with octahedral covalent bonding shows a very small temperature dependence of the quadrupole splitting: it is of the order of <0.01 (mm/sec)/100°.

For closed electron shells or half-shells, and with almost no effect due to the remaining crystal lattice, the splitting is given by the charge distribution on the ion, complex ion, or molecule in question. An over-all picture of possible splittings is obtained from simple symmetry considerations. It is $\epsilon = 0$ if there are at least two 3- or more-fold rotational axes (3-fold or more), and $\eta = 0$ if there is only one such axis. The field gradient will not be altered if a charge is mirrored at the center. Accordingly for $[Fe^{II}(CN)_6]^{4-}$ a value of $\epsilon = 0$ is to be expected, and for the prussiates, in which CN groups are replaced by another ligand, $\epsilon \neq 0$ and $\eta = 0$. In $[Fe^{II}(dipyridyl)_3]^{2+}$, in which iron also uses octahedral d^2sp^3 orbitals in bonding, there is no strictly 3-fold axis because of the bidentate nature of the ligands, and a small splitting is to be expected. For $Fe(CO)_5$, which forms a trigonal bipyramid, there is only one 3-fold axis and thus $\epsilon \neq 0$ and $\eta = 0$ is to be expected. If iron d^3s orbitals are used in forming the σ-bonded structure of $[Fe^{VI}O_4]^{2-}$, which follows from the lack of splitting and from the value of δ, the $3d$ half-shell which does not participate in the

hybridization is closed. The value of ϵ should then be zero because of the tetrahedral symmetry. In $[Fe^{III}S_2]^-$ and $[Fe^{III}O_2]^-$ with sp^3 configurations, the chain structure of the anion should give rise to a small splitting. All these expectations are fulfilled, as may be seen from a glance at the table. Thus values of ϵ may be predicted reasonably well.

d. Bond Character. Like the values of the quadrupole splitting, those of the isomer shift are characteristic of the way in which iron is bonded. The ideas on the relationship between isomer shifts and s electron densities, which were developed by Walker *et al.*, have already been mentioned (p. 454). The values of δ, measured by us, referred to Co^{57} in platinum as a radiation source and those expected for configurations from $3d^4$ to $3d^8$ are shown in Fig. 37.

In Fig. 37, $[Fe^{VI}O_4]^{2-}$ has the highest s electron density at the nucleus of iron. For this ion, bonds based on sp^3 or d^3s hybrids could be assumed. The first possibility can, however, be discarded at once, for with the $3d^2$ configuration and a $4s$ contribution, a considerably greater s electron density would be expected (see Fig. 13). The absence of quadrupole splitting leads to the same conclusion. There must therefore be d^3s hybridization. If, in keeping with the model of the donor bond, one electron of iron is included in each of the four hybrid orbitals so that the formal configuration $3d^54s^1$ results, one obtains the right order of magnitude for the shift, the observed value of which lies between $3d^5$ and $3d^4$. The greater s electron density compared with $3d^5$ is to be explained in terms of the $4s$ contribution.

As a first approximation the rough picture of bonding which has already been employed is useful. The application of more exact functions for the $3d^n4s^m$ configurations, which take account, for example, of $4s$-$3s$ screening, and also the consideration, in part at least, of the actual bonding hybrid functions, should result in considerable improvement in the calculation of line shifts, δ. Probably the components of the hybrid functions may be replaced to a good approximation by the components of the functions from which the hybrid functions are formed by linear combination, though the orbitals concerned must then be occupied in a suitable way. Using first the simplified picture of the covalent bond, where one electron of the bonding orbital is assigned to iron, one has, in place of the full occupation of one spin direction, half occupation of both spin directions. In general, this leads in the case of a $3d$ orbital to a somewhat stronger screening of the $3s$ electrons and, in the case of the $4s$ orbital, to a somewhat larger contribution to the s electron density.

The line shifts of iron bonded in a complex all fall in the same range irrespective of the formal oxidation number, as may be seen from Figs. 12 and 37. Metallically bonded iron also falls in just the same range. To explain this phenomenon we must recall the Pauling electron neutrality principle,

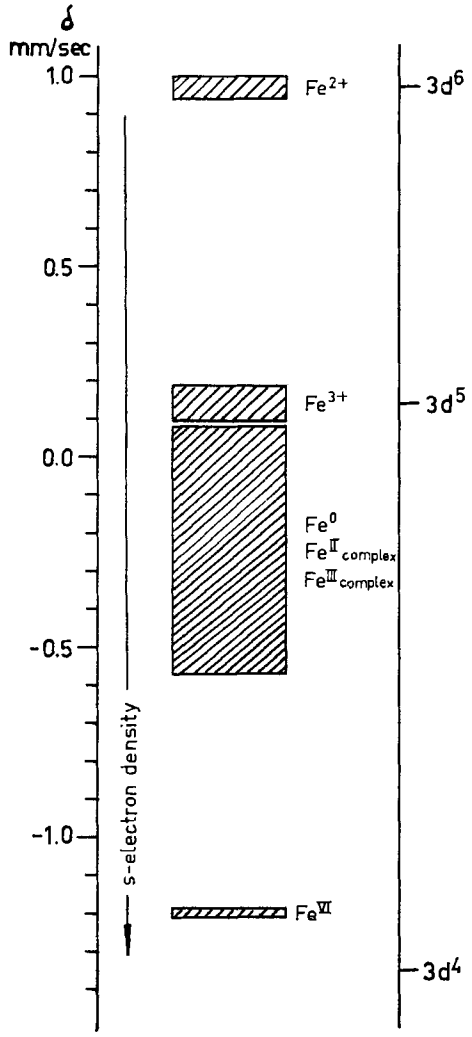

FIG. 37. Characteristic ranges for the shift δ with theoretical values for the configuration $3d^n$.

according to which the charge adjusts itself between the central atom and its covalently bonded ligands in such a way that the effective charge on the central atom remains between -1 and $+1$. This charge adjustment may be brought about in many cases by π-bonds, which occur in addition to σ-bonds. In other cases, however, as for example for $[FeO_4]^{2-}$ with O^{2-} ligands, this mechanism is impossible. In such circumstances charge adjustment is brought about by increase in the ionic component of the σ-bond.

Where possible, relatively strong π-bonds occur in addition to σ-bonds in all the complexes considered. These are formed between the 3 orbitals of iron which are not involved in σ-bonding and suitable orbitals of the ligands. In this way $3d$ electrons and the s electron density at the nucleus increase. For Fe^0 with dsp^3 bonding four π-bonds are possible, while for $Fe^{II}(d^2sp^3)$ three and for $Fe^{III}(d^2sp^3)$, because of the missing electron, only two π-bonds can be formed. With maximum π-bond formation there are in all three cases five $3d$ electrons and a decrease of the formal charge to -1. This explains the practically identical δ values for $[Fe(CN)_6]^{4-}$ and $[Fe(CN)_6]^{3-}$. The fact that $Fe(CO)_5$ shows almost the same δ value may be understood in terms of the stronger π-bonding of CO ligands compared with CN^- ligands.

From the δ values of metallically bonded iron in Table II it follows that, with the introduction of metals which are more electronegative than iron, the s electron density at the iron nucleus becomes smaller. Introduction of more positive metals causes it to increase as is shown, for example, by the values for Cr and Mn given by Walker *et al.* (*52*). On the whole, δ values vary in accordance with Pauling's scale of electronegativities. More electropositive metals withdraw more $4s$ electrons from iron, as indeed would be expected. In place of the effective $3d^74s^1$ configuration of metallic iron, which has been variously proposed, the configuration $3d^64s^x$ with $x > 1$ seems to us to be more suitable since the $4s$ electrons play the chief role, according to what has been said. Occupation of the $3d$ levels by more than six electrons is also less probable.

Relatively small line shifts δ are, however, attributable to the isomer shift if the differences due to the influence of the crystal lattice on the isomer shift and the differences of the temperature shift are sufficiently small. These small differences may be used to determine the relative strengths of bonding of the various ligands, although absolute values for the strength of the π-bond cannot be given directly.

The prussiates, for example, are especially suitable for these investigations. If the new ligand establishes a stronger π-bond with the iron than CN^-, the $3d$ occupation is reduced and one obtains a bigger s electron density at the iron nucleus and a positive field gradient. Correspondingly, a weaker π-bond gives a lower s electron density and a more negative field gradient. Since the field gradient disappears in $[Fe(CN)_6]^{4-}$, one has with stronger π-bonding the field gradient of a positive, and with weaker π-bonding that of a negative charge distribution in the direction of the substituents. A review of the behavior of various substituents for the CN^- group in $[Fe(CN)_6]^{4-}$ is given in Section III,B,*8*,*b*.

In principle, analogous investigations may also be made for $Fe(CO)_5$. Similar relationships would be expected when a CO group is replaced, i.e.,

for weaker π-bonding components of the new ligands a smaller s electron density may be anticipated. Because of the different symmetry the behavior of the field gradient will, however, be different from that for prussiates. An over-all description is given by a simple model: negative charge is withdrawn in the direction of the bond from the spherosymmetrical charge distribution $3d^{10}4sp^3$. The field gradient corresponds to that in the center of a trigonal bipyramid at the corners of which there are equal positive charges at the same distance from the center. This gives a large positive field gradient, as is observed for $Fe(CO)_5$. If a π-bond is removed, this means that the positive charge at one corner of the bipyramid is reduced. The field gradient will become zero if this positive charge decreases to half its initial value and will become negative on further reduction. Depending on the strength of the π-bond which is removed, the field gradient may become smaller or even negative. The values of δ and ϵ for the compound $Fe(CO)_4I_2$, which results when one CO group in $Fe(CO)_4$ is substituted by I_2, are in good agreement with this conception. No π-bond is formed in this case between I_2 and Fe because the $5p$ and $5d$ orbitals of iodine are too diffuse for a bond.

10. Mössbauer Spectroscopy of Sn^{119}

As may be seen from the data in Table I, the isotope Sn^{119} should be very suitable for studying the Mössbauer effect. γ-Quanta of 24-kev energy are emitted in the transition from the first excited state to the ground state. The conversion coefficient α is 7.3. It follows from the Doppler theory that the energy ΔE with a relative velocity v of source and absorber is $\Delta E = (v/c)E$ with E being the γ-ray energy, i.e., for a 24-kev γ-quantum, 8×10^{-8} ev per cm/sec.

A large number of tin compounds were investigated by Kistner and associates (*28*). The observed isomer shifts and quadrupole splittings are shown in Table VII. The isomer shifts relate to a white tin source and fall in three regions which appear to be characteristic of Sn^{2+} and Sn^{4+} compounds and of tin in alloys.

In interpreting the observed shifts, the authors related them to the most probable electron configurations of tin in these compounds. The ordinate in Fig. 38 shows the number of $5p$ electrons of the tin, while the abscissa gives the number of $5s$ electrons. Starting from the assumption that the sp^3 configuration is present in gray tin or that the sum of the s and p electrons is 2 for compounds in which tin has an oxidation number of $+2$, (i.e., the shifts lie on the line $s + p = 2$, and mainly in the region of $s = 2$), there are a number of regions in the diagram in which the members of the various classes of compound should fall. Compounds of tin in which it has an oxidation number of $+4$ should fall in a region which lies to the right

TABLE VII
ISOMER SHIFTS AND QUADRUPOLE SPLITTINGS OF Sn^{119}

Compound	δ (mm/sec)	ϵ (mm/sec)
SnF_2	+0.85	1.58
$SnCl_2 \cdot 2H_2O$	+1.09	1.24
$SnBr_2$	+1.38	—
$SnSO_4$	+1.41	0.90
SnO	+0.13	1.30
SnS	+0.85	1.13
SnF_4	−2.77	2.03
$SnCl_4 \cdot 5H_2O$	−2.26	—
$SnBr_4$	−1.32	—
SnI_4	−1.19	—
$Sn(SO_4)_2 \cdot 2H_2O$	−2.82	—
SnO_2	−2.54	—
SnS_2	−2.23	0.80
Mn_4Sn	+0.70	—
Sn in Fe, Ni, Co	−1.00	—
$SnNb_3$	−1.00	—
SnV_3	−0.98	—
Sn_2Ir	−0.79	—
SnPt	−0.65	—
SnAu	−0.18	—

of the point $s = 0$, $p = 0$; in these a small total number of electrons is to be expected. That this total number is not equal to zero expresses the fact that the bond is covalent to some extent in character in these tin(IV) compounds. Kistner *et al.* have tentatively drawn in the diagram lines of constant isomer shift, i.e., of constant s electron density on the nucleus. The straight lines run almost parallel to the ordinate, from which it may be deduced that the p electrons do not screen the s electrons to any considerable extent.

Detailed studies of tin compounds have also been carried out by Goldanski *et al.* (*14a*).

IV. Prospect

An attempt has been made in the foregoing pages to describe the nature of the Mössbauer effect and its significance in chemistry. Looking back on what has been said in the various sections about the conclusions reached with the aid of the Mössbauer effect on the structure of iron compounds and the nature of the bonding, it is probably true to say that Mössbauer spectroscopy is no less fruitful than other physical methods. Moreover, it is able to solve problems which, in many cases, other methods are unable to answer. The study of other compounds will clarify many points where,

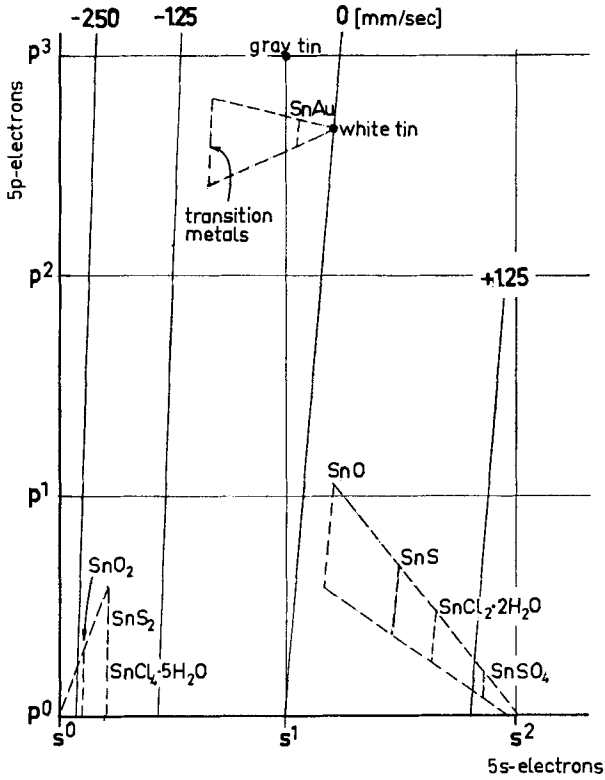

FIG. 38. Schematic coordination of isomer shifts in Sn(II) and Sn(IV) compounds and in Sn alloys (*28*).

at the moment, because of the relatively small amount of empirical information, only speculation is possible. Further progress will also doubtless come from the extension of the measurements to the nuclei of other elements. Even if Mössbauer spectroscopy, because of the lack of suitable isotopes, is incapable of application to all areas of chemistry—and this is true of almost every method—it will be able in many cases to contribute to the solution of chemical problems.

ACKNOWLEDGMENT

The author gratefully acknowledges the permission granted by Verlag Chemie to reproduce portions of an article originally published in *Angewandte Chemie* International Edition, Volume 2, No. 6, 1963.

REFERENCES

1. Barloutaud, R., Picou, J. L., and Tzara, C., *Compt. Rend.* **250,** 2705 (1960).
2. Boyle, A. J. F., Bunbury, D. St. P., and Edwards, C., *Proc. Phys. Soc. (London)* **76,** 165 (1960).

3. Brady, P. R., Wigley, P. R. F., and Duncan, J. F., *Rev. Pure Appl. Chem.* **12,** 165 (1962).
4. Burns, G., *Phys. Rev.* **123,** 1634 (1961).
5. Cohen, M. H., and Reif, F., *Solid State Phys.* **5** (1957).
6. Dahl, L. F., and Rundle, R. E., *J. Chem. Phys.* **26,** 1751 (1957); see also *J. Chem. Phys.* **27,** 323 (1957).
7. Das, T. P., and Hahn, E. L., *Solid State Phys. Suppl.* **1,** (1958).
8. De Benedetti, S., Lang, G., and Ingalls, R., *Phys. Rev. Letters* **6,** 60 (1961).
9. De Coster, M., Pollak, H., and Amelinckx, S., *Phys. Stat. Sol.* **3,** 283 (1963).
10. Emeléus, H. J., and Anderson, J. S., "Modern Aspects of Inorganic Chemistry," 2nd ed. Routledge and Hegan Paul, London, 1952.
11. Ewens, R. V. G., and Lister, M., *Trans. Faraday Soc.* **35,** 681 (1939).
12. Fermi, E., and Segrè, E., *Z. Physik* **82,** 729 (1933).
13. Fluck, E., Kerler, W., and Neuwirth, W., *Angew. Chem.* **75,** 461 (1963).
14. Frauenfelder, H., "The Mössbauer-Effect." W. A. Benjamin, New York, 1962.
14a. Goldanskii, V. N., *et al.*, *Proc. Acad. Sci. USSR* **147,** 127 (1962); *Zh. Eksperim. i Teor. Fiz.* **22,** 637 (1962); **43,** 448 (1962); **44,** 752 (1963); *Atomic Energy Review* **1,** No. 4 (1963).
15. Goudsmit, S. A., *Phys. Rev.* **43,** 636 (1933).
16. Hanna, S. S., Preston, R. S., and Heberle, J., *in* "Proceedings 2nd International Conference on the Mössbauer-Effect" (D. M. J. Compton and A. H. Schoen, eds.), p. 85. Wiley, New York, 1962.
17. Hanna, S. S., Heberle, J., Littlejohn, C., Perlow, G. J., Preston, R. S., and Vincent, D. H., *Phys. Rev. Letters* **4,** 177 (1960).
18. Herber, R. H., Kingston, W. R., and Wertheim, G. K., *Inorg. Chem.* **2,** 153 (1963).
19. Johnson, C. E., Marshall, W., and Perlow, G. J., *Phys. Rev.* **126,** 1503 (1962).
20. Josephson, B. D., *Phys. Rev. Letters* **4,** 341 (1960).
21. Kalvius, M., Zahn, U., Kienle, P., and Eicher, H., *Z. Naturforsch.* **17a,** 494 (1962).
22. Keggin, O. F., and Miles, F. D., *Nature* **137,** 577 (1936).
23. Kerler, W., *Z. Physik* **167,** 194 (1962).
24. Kerler, W., and Neuwirth, W., *Z. Physik* **167,** 176 (1962).
25. Kerler, W., Neuwirth, W., and Fluck, E., *Z. Physik* **175,** 200 (1963).
26. Kerler, W., Neuwirth, W., Fluck, E., Kuhn, P., and Zimmermann, B., *Z. Physik* **173,** 321 (1963).
27. Kistner, O. C., and Sunyar, A. W., *Phys. Rev. Letters* **4,** 412 (1960).
28. Kistner, O. C., Jaccarino, V., and Walker, L. R., *in* "Proceedings 2nd International Conference on the Mössbauer Effect" (D. M. J. Compton and A. H. Schoen, eds.), p. 264 Wiley, New York, 1962.
29. Knight, W. D., *Phys. Rev.* **76,** 1259 (1949).
30. Lamb, W. E., *Phys. Rev.* **55,** 190 (1939).
31. Margulies, S., and Ehrmann, J. R., *Nucl. Instr. Methods* **12,** 131 (1961).
32. Mills, D. S., *Chem. Ind.* (*London*) p. 73 (1957).
33. Mössbauer, R. L., *Z. Physik* **151,** 124 (1958).
34. Mössbauer, R. L., *Naturwissenschaften* **45,** 538 (1958).
35. Mössbauer, R. L., *Z. Naturforsch* **14a,** 211 (1959).
36. Moon, P. B., *Proc. Phys. Soc.* (*London*) **A64,** 76 (1951).
37. Moon, P. B., and Storruste, A., *Proc. Phys. Soc.* (*London*) **A66,** 585 (1953).
38. Nagle, D. E., Frauenfelder, H., Taylor, R. D., Cochran, D. R. F., and Matthias, B. T., *Phys. Rev. Letters* **5,** 364 (1960).

39. Orgel, L. E., "An Introduction to Transition-Metal-Chemistry: The Ligand-Field Theory." Methuen, London, 1960.
40. Pollak, H., De Coster, M., and Amelinckx, S., *Phys. Stat. Sol.* **2,** 1653 (1962).
41. Pound, R. V., and Rebka, G. A., Jr., *Phys. Rev. Letters* **4,** 337 (1960).
42. Pound, R. V., and Rebka, G. A., *Phys. Rev. Letters* **4,** 274 (1960).
43. Powell, H. M., and Ewens, R. V. G., *J. Chem. Soc.* p. 286 (1939).
44. Preston, R. S., Hanna, S. S., and Heberle, T., *Phys. Rev.* **128,** 2207 (1962).
45. Robin, M. B., *Inorg. Chem.* **1,** 337 (1962).
46. Ruby, S. L., Epstein, L. M., and Sun, K. H., *Rev. Sci. Instr.* **31,** 580 (1960).
47. Shirane, G., Cox, D. E., and Ruby, S. L., *Phys. Rev.* **125,** 1159 (1962).
48. Shirley, D. A., *Phys. Rev.* **124,** 354 (1961).
49. Solomon, J., *Compt. Rend.* **250,** 3828 (1960).
50. Sternheimer, R. M., *Phys. Rev.* **80,** 102 (1950).
51. Sternheimer, R. M., and Foley, H. M., *Phys. Rev.* **102,** 731 (1956).
52. Walker, L. R., Wertheim, G. K., and Jaccarino, V., *Phys. Rev. Letters* **6,** 98 (1961).
53. Watson, R. E., and Freeman, A. J., *Phys. Rev.* **123,** 2027 (1961).
54. Wertheim, G. K., *Phys. Rev.* **121,** 63 (1961).
55. Wertheim, G. K., and Herber, R. H., *J. Chem. Phys.* **38,** 2106 (1963).
56. Winkler, H. G. F., "Struktur und Eigenschaften der Kristalle." Springer, Berlin, 1955.
57. Wyckoff, R. W. G., "Crystal Structure," Wiley (Interscience), New York, 1960
58. Zahn, U., Kienle, P., and Eicher, H., *Z. Physik* **166,** 220 (1962).